

**A Thesis Submitted for the Degree of PhD at the University of Warwick**

**Permanent WRAP URL:**

<http://wrap.warwick.ac.uk/157003>

**Copyright and reuse:**

This thesis is made available online and is protected by original copyright.

Please scroll down to view the document itself.

Please refer to the repository record for this item for information to help you to cite it.

Our policy information is available from the repository home page.

For more information, please contact the WRAP Team at: [wrap@warwick.ac.uk](mailto:wrap@warwick.ac.uk)

# **SYNTHESIS AND MODIFICATION OF CALCIUM CARBONATE MICROPARTICLES AND THEIR USE AS ABRASIVES IN TOOTHPASTE**

**Patrik Karl Albert Olsson**

**A dissertation presented in fulfilment of the requirements for the  
degree Master of Philosophy in Chemistry**

**Department of Chemistry**

**University of Warwick**

**July 2020**

# TABLE OF CONTENTS

ACKNOWLEDGEMENTS .....	iv
DECLARATION .....	v
ABSTRACT.....	vi
CHAPTER 1 “General Introduction” .....	1
1.1 Introduction .....	2
1.2 Layout of dissertation.....	3
CHAPTER 2 “Calcium carbonate particles synthesised in linear polyol containing media” ....	4
2.1 Introduction .....	5
2.1.1 Calcium carbonate overview .....	5
2.1.2 Effect of alcohol moieties on precipitated calcium carbonate.....	8
2.2 Experimental Section .....	10
CaCO <sub>3</sub> synthesis via direct precipitation.....	11
CaCO <sub>3</sub> synthesis via ureolysis.....	12
CaCO <sub>3</sub> synthesis via vapour diffusion.....	12
2.3 Results and Discussion.....	13
2.3.1 Effect of polyol length on morphology of CaCO <sub>3</sub> .....	13
2.3.2 Effect of reaction time on CaCO <sub>3</sub> particle morphology .....	16
2.3.3 Effect of temperature on CaCO <sub>3</sub> particle morphology .....	18
2.3.4 Effect of glycerol concentration on CaCO <sub>3</sub> particle morphology .....	18

2.3.5 CaCO <sub>3</sub> synthesised via vapour diffusion.....	20
2.3.6 Effect of glycerol concentration on CaCO <sub>3</sub> formed by ureolysis.....	20
2.4 Conclusions .....	21
CHAPTER 3 “Calcium carbonate particles as templates for synthesis of hybrid microparticles” .....	22
3.2 Experimental Section .....	23
Polymer coating of calcium carbonate particles (polymer@CaCO <sub>3</sub> ).....	23
Calcium carbonate to calcium fluoride conversion (CaF <sub>2</sub> @CaCO <sub>3</sub> ) .....	23
Silica coating of calcium carbonate particles (SiO <sub>2</sub> @CaCO <sub>3</sub> ).....	23
Formation of magnetite on acid functionalised hollow polymer shell .....	24
Dissolution of CaCO <sub>3</sub> from polymer@CaCO <sub>3</sub> , CaF <sub>2</sub> @CaCO <sub>3</sub> , and SiO <sub>2</sub> @CaCO <sub>3</sub> .....	24
3.3 Results and Discussion.....	25
3.3.1 Polymer coating of CaCO <sub>3</sub> particles.....	25
3.3.2 Silica coating of CaCO <sub>3</sub> particles .....	28
3.3.3 Conversion of CaCO <sub>3</sub> particles to CaF <sub>2</sub> .....	32
3.3.4 Magnetite formation on acid-functionalised hollow polymer shells .....	35
3.4 Conclusions .....	36
CHAPTER 4 “Testing cleaning ability of microparticles” .....	38
4.1 Introduction .....	39
4.1.1 Background to oral care .....	39
4.1.2 Toothpaste design.....	40

4.1.3 Evaluation of dentifrice performance .....	43
4.2 Experimental Section .....	43
4.3 Results and Discussion.....	45
4.4 Conclusions .....	51
CHAPTER 5 “Conclusions and Future Recommendations” .....	52
General conclusions .....	53
Recommendations .....	53
MATERIALS AND ANALYTIC METHODS .....	54
Materials.....	54
Analytic methods.....	54
REFERENCES .....	56

---

## ACKNOWLEDGEMENTS

I would like to thank my sponsor, Unilever, for the opportunity to work on this project.

A massive thank you to Stefan Bon, my supervisor, for all his support throughout my years working in his labs.

To all lab members I have worked with over the years, thank you for your camaraderie. We have shared beers, laughs and more beers. I am sure we will share many more in the future.

To the various staff, academics, and students at Warwick, who are far too many to mention, thank you helping me out over the years, whether it be showing me how to use a piece of equipment or asking for a door code for the umpteenth time.

To my family, and especially my parents, thank you for your support throughout my life. I am lucky to have you in my life.

Chris, when times were at their lowest you were there for me unconditionally. I love you man.

Abbie, without you I would never have even started writing this dissertation, and for that I thank you from the bottom of my heart.



## DECLARATION

I declare that the entirety of the work contained herein is my own original work (unless explicitly specified), and that I have not previously, in part or in its entirety, submitted it for obtaining any other qualification. All work presented was carried out in the laboratories of University of Warwick and Unilever Port Sunlight.

*Chapter 4* – Particles synthesised by Christopher Parkins and Robert Young were used for cleaning tests. Christopher Parkins aided with performing cleaning tests.

Patrik Karl Albert Olsson

July 2020



## ABSTRACT

Use synthesis of calcium carbonate particles, and their use as templates for further modification, with the aim of their use as abrasives in toothpaste formulations, is explored in this dissertation. Linear polyols were shown to have a strong affect on the morphology of precipitated calcium carbonate particles, as well as a stabilizing effect of the vaterite polymorph. Calcium carbonate particles were successfully coated with silica via a condensation reaction, as well as in polymer via a seeded dispersion polymerization. Calcium carbonate particles were used as sacrificial templates to produce calcium fluoride particles with the same morphology as the template. Synthesised particles were shown to have tooth cleaning abilities similar to commercially used abrasive particles, but significant conclusions regarding how their morphology affected this could not be drawn due to unreliable data.





# **CHAPTER 1**

## **“General Introduction”**


In this chapter the motivation for the research is explained. The use of microparticles as abrasives in toothpaste is introduced. The layout of the dissertation presented.

## 1.1 Introduction

The use of colloidal particles of the nano- and micrometer scale is proliferate within many applications such as bulk material design, catalysis, and diagnostics. Organic, inorganic, and polymeric chemistries provide a wide range of mechanical and reactive functions which can serve as tools in tailoring particles for specific uses as abrasives, capsules, catalytic reactors, pigments, and much more.<sup>1-4</sup> The ability to control properties such as material, morphology, and surface functionality allows their performance to be tailored for its intended use. Additionally, because of legal and moral restrictions due to health and ecological concerns, it is vital that research into new particles which adhere to these restrictions is undergone.<sup>5</sup> Calcium carbonate is a mineral found extensively throughout nature, being present in geological rock formations as well as a major component in biological structures such as shells. Within industries such as paint-, plastic-, and papermaking it is widely used as a filler due to its low cost and wide abundance.

The application of inorganic particles which this work concerns itself particularly with is their use as abrasives in dentifrices, products which are used to clean teeth. Factors such as material hardness, particle morphology and size affect the cleaning and damaging properties of abrasives. Restrictions such as cost and biocompatibility of materials limit the range of particles that could be used for the application, with calcium carbonate and silica based abrasives making up the majority of those used commercially.

This research was initially based on comparing how effective micron sized particles of different morphologies are as abrasives in toothpaste formulations, with the desire to find particles with high cleaning ability whilst causing little damage to the underlying tooth surface. Of particles examined, elongated (rod-like) calcium carbonate microparticles became of particular interest, and then played a central theme to further experimentation. Explored are the novel syntheses



of various morphologies of calcium carbonate particles using a range of reaction conditions. These particles were then used as hard templates for the surface addition of other materials, such as silica polymers, to form hybrid core-shell particles. The transformation of calcium carbonate particles to calcium fluoride with morphology retention was examined. Finally, the cleaning ability of synthesized particles was examined to evaluate their potential use as abrasives in toothpaste.

## **1.2 Layout of dissertation**

### **Chapter 2**

This chapter explores the syntheses of various calcium carbonate particles using linear polyols as crystal growth modifiers.

### **Chapter 3**

This chapter shows the modification of calcium carbonate particles via surface addition of polymers and silica, as well as the transformation into calcium fluoride particles.

### **Chapter 4**

This chapter presents cleaning results of various inorganic particles as abrasives in toothpaste.

### **Chapter 5**

This chapter summarises all the work and presents recommendations for further investigations.



## **CHAPTER 2**

### **“Calcium carbonate particles synthesised in linear polyol containing media”**

In this chapter novel syntheses which produce a range of calcium carbonate particle morphologies are presented. The effect which reaction solvent composition, along with other factors, have on these synthesised particles, are discussed.

## 2.1 Introduction

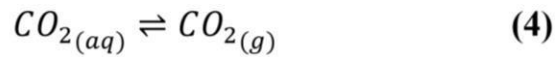
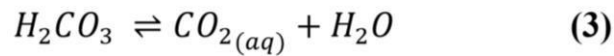
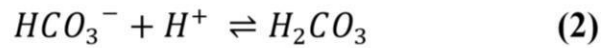
With the aim of producing microparticles to be used as abrasives in toothpaste, calcium carbonate was chosen as the material due to its prevalent use and range of obtainable morphologies. In this chapter the synthesis of calcium particles is explored, with a focus on using linear polyols as crystallization modifiers to affect particle morphology.

### 2.1.1 Calcium carbonate overview

Crystallisation is the overarching term used to describe the nucleation and growth of crystalline solid phases.<sup>5</sup> Classical nucleation theory describes the initial formation of a new crystalline phase.<sup>5,6</sup> The driver for this is a decrease in free energy from the formation of the new phase decreasing the saturation of the mother solution, scaling with the volume of the particle. However, the formation of a new phase comes at the energetic cost of surface tension between the mother solution and new crystalline phase. At small particle sizes the surface tension energetics dominate, and as a result, most formed proto-crystals redissolve into solution. Some particles overcome this energy barrier, reaching a critical particle, after which the bulk energy term dominates and the now stable crystal proceeds to grow. Crystal growth involves the addition of monomeric species in a supersaturated solution to a growing particle due to the difference in chemical potential between the particle and the solution. Classical nucleation does not account for observations made in numerous systems, for example those which exhibit multiple crystallization pathways towards reaching a thermodynamically stable state.<sup>6-9</sup>

Calcium carbonate ( $\text{CaCO}_3$ ) has received copious academic and industrial interest due to its natural abundance, wide range of applications, and richness of available morphologies.<sup>10</sup> The role of calcium carbonate as an atmospheric carbon dioxide regulator makes it unique with the importance of having its equilibria maintained to avoid major disruption to many ecosystems. Shown below are the equilibria of the processes between carbon dioxide in the atmosphere dissolving in water, to the formation of calcium carbonate from its reaction with

dissolved calcium ions.<sup>11</sup>




It is important to note that as the effective  $pK_a$  of carbonic acid is 6.3 at standard conditions, even mildly acidic conditions will create a thermodynamic drive to protonate the carbonate ion, with the knock-on effect of calcium carbonate dissolving to maintain equilibrium. In nature and society this implies an issue as increased acidity of the oceans due to elevated atmospheric carbon dioxide levels greatly increases the solubility of various animal structures and reefs which could decimate connected ecosystems. In the laboratory this makes working with calcium carbonate difficult in some respects as acidic environments will readily dissolve any calcium carbonate.

Calcium carbonate exists mainly as one of three crystalline polymorphs: calcite, aragonite, and vaterite, in order of most to least stable, with respective solubility products ( $\log K_{sp}$ ) of -8.48, -8.34, and -7.91.<sup>12</sup> Calcite is the most naturally abundant polymorph and is the form which all other polymorphs eventually turn into through recrystallisation. Aragonite is mainly found within aquatic biominerals where high magnesium ion concentrations, amongst other factors, aid its formation. Although less stable aragonite can take up to the order of 100 million years to fully convert to calcite based on fossil evidence.<sup>13</sup> Vaterite is the least stable of the three and rarely exists in nature without being stabilised by proteins or other chemical species.<sup>14</sup> Another form of calcium carbonate, amorphous calcium carbonate (ACC), is a highly hydrated gel-like amorphous material which acts as a precursor to the crystalline polymorphs and rarely exists for more than seconds or minutes.<sup>15</sup> Another polymorph, monohydrocalcite, exists but is formed by a limited number of organisms. Calcium carbonate hexahydrate, known also as ikaite, is not yet known to be produced in nature.<sup>16</sup>

Ostwald's rule states that the least stable polymorph will tend to be the first to appear during crystallization of a melt or solution.<sup>17</sup> Kinetically, the more soluble form is preferentially formed due to a lower interfacial energy between the mineral and solution.<sup>18</sup> In the case of calcium carbonate which is homogeneously precipitated this initial polymorph is ACC. When calcium and carbonate ions are present in a high enough concentration together in solution a supersaturation with respect to calcium carbonate thermodynamically drives its precipitation, forming a new solid phase. Initially ACC will be formed and afterwards, depending on reaction conditions, proceeds to crystallise to one of the other crystalline polymorphs. Given time all calcium carbonate will recrystallise to calcite, but the order in which this occurs is not as simple as ACC to vaterite to aragonite to calcite. Studies have shown ACC crystallising to calcite or aragonite without vaterite being present as a middle step, and vaterite transforming to calcite without aragonite being present.<sup>19-21</sup>

The fact that there is no overwhelmingly regular order in which these transformations between polymorphs occurs gives support to the idea that the crystallisation and recrystallisation events are highly affected by the environment outside of the crystal, and not occurring by a solid-state recrystallisation mechanism. Dissolution-recrystallisation is a mechanism which has been postulated and supported in many systems, whereby small amounts of the less stable polymorph dissolves on the crystal edge and then crystallises back onto the same mass as a more stable polymorph.<sup>21-23</sup> Although solid-state recrystallisation mechanisms on the surface of crystal grains can occur, these are likely to play a less significant role compared to the dissolution-reprecipitation mechanism in solvated calcium carbonate systems due to the relatively high energy barrier.<sup>24</sup> In contrast to the recrystallisation between crystal polymorphs, the initial crystallization of ACC appears to occur with a more complicated combination of dissolution-reprecipitation and solid-state transformation, during which water is expelled from the material.<sup>25-27</sup>

ACC has been shown to be an important precursor in the crystal phases of biological organisms,



which use it as temporary storage deposits.<sup>28</sup> Compared to its crystalline counterparts, ACC is more soluble and has a highly disordered structure which can be moulded into different shapes.<sup>29</sup> The ACC crystallisation pathway is adopted by many biomineralising organisms when forming their shells and/or spines in order to control the particle shape and crystalline morphology of the material. These biogenic processes have provided an insight into the realisation of a biomimetic strategy for controlled crystallisation and are used to manipulate the abiotic synthesis of calcium carbonate. The chemistry and structure of ACC is complex, with several forms being classified according to their water content and mode of formation (i.e. biogenic or abiotic).<sup>21</sup> Beniash et al. reported that ACC acted as a seed for the growth of other polymorphs, with ACC present in the initial stages of crystal growth, transforming into calcite over time.<sup>30</sup>

In the laboratory various morphologies of calcium carbonate particles have been synthesised, from hexagonal plates and spheroids to more chrysanthemum flower shapes.<sup>31–33</sup> Some of the structures found in nature overshadow their synthetic counterparts in complexity, such as the regularly arranged hexagonal platelets in nacre (mother of pearl) which act as a colloidal crystal, creating its hallmark iridescence.<sup>34</sup> Biological calcium carbonate has also shown to have superior properties, such as increased toughness hardness, compared to that from synthetic sources.<sup>35</sup> These differences between biological calcium carbonate and that available from current synthetic methods are due largely to the precise use of additive species like polysaccharides and proteins.<sup>36</sup> The possibilities of architectures and properties shown by natural calcium carbonate, as well as other minerals, has provided inspiration for the further understanding of crystallization, and development of more advanced synthetic materials.

Many factors influence the nucleation, growth, and transformation steps of the crystallization process, such as the temperature, supersaturation of the crystalline material, reaction pH, and the presence of additives which may be only surface active during crystallization or occluded within the crystal matrix itself.<sup>10,23,37,38</sup> Other experimental conditions like stirring rates, the



fashion in which reactants are added, and the use or absence of seed crystals likewise affect the outcomes of crystal synthesis.<sup>37,39</sup> Changing any of these reaction conditions can lead to large effects on polymorph selection, particle size, morphology, and whether a single crystal or polycrystalline material is obtained.<sup>40–42</sup>

### ***2.1.2 Effect of alcohol moieties on precipitated calcium carbonate***

Several studies have shown that molecules containing alcohol moieties exhibit a strong effect on polymorph selection and morphology of precipitated calcium carbonate particles. Stipp et al. precipitated calcium carbonate with varying amounts of ethanol, 1- and 2-propanol, along with varying agitation rates, and was able to produce a large variety of particle morphologies.<sup>43</sup> Additionally when 10 vol% alcohol were used almost all particles had a high level of calcite polymorphism, whilst when 50 vol% alcohol was used the majority of particles were dominantly aragonite and/or vaterite. In the system Dalas and Manoli used high amounts of vaterite particles were formed even when 10 vol% alcohol was used, however this could be partially attributed to the initial reaction solution having its pH adjusted up to 8.5.<sup>44</sup> Youmeng et al. found that in their system they initially produced small agglomerates of calcium carbonate when in pure water, which transitioned to large flower shaped vaterite particles with 80% ethanol content, with the particles at 50% showing a similarly shaped but ‘damaged’ vaterite flowers mixed with calcite.<sup>33</sup> In a similar vein a paper by Chen et al. showed that by increasing the concentration of ethanol in their system the polymorphic distribution of precipitated calcium carbonate went from a combination of aragonite and vaterite, to pure aragonite, to a mixture of vaterite and aragonite, and finally almost pure vaterite in the highest ethanol containing solution.<sup>41</sup> Li et al. proposed that alcohol groups in polyols adsorbed onto growing vaterite nuclei to lower their surface energy and make the phase thermodynamically more stable than other phases, resulting in the precipitation of relatively pure vaterite.<sup>45</sup>

Polymeric molecules containing alcohol groups have also shown to exhibit similar stabilising

effects. Kim et al. used several polymers in their system and found that when poly(vinyl alcohol) was used the vaterite phase was stabilised from transforming into calcite for nearly two days, whilst when non-alcohol containing polymers were used the transformation proceeded to 90% within one hour.<sup>46</sup> Additionally when higher amounts of PVA were used, the vaterite transformed into aragonite as opposed to calcite. Hosoda and co-workers found the addition of PVA caused their films of calcium carbonate to form vaterite, whereas when it was withheld aragonite was formed.<sup>47</sup>

Another study by Stipp et al. showed through XPS measurements and molecular dynamic simulations that when different single alcohol containing molecules with varying sizes of alkyl chains (methanol, ethanol, pentanol, and t-butanol) were introduced to calcite surfaces all of the molecules bound through the alcohol group and formed well-ordered monolayers on the surface.<sup>48</sup> Whilst this study only concerns the calcite polymorph, and does not hint towards any stabilising effect of the other phases, it shows the strong interaction which alcohol groups exhibit towards calcium carbonate surfaces. Whilst all these studies paint a complicated picture of the effect which alcohol groups have on growing calcium carbonate particles, there appears to be a general theme that alcohols decrease the formation of calcite, and specifically increase the appearance of vaterite.

The avenue of research into the effect which polyols have on synthesised calcium carbonate particles, which part of this dissertation is dedicated to, was inspired in part by a paper by Trushina et al..<sup>49</sup> In it they looked at how various parameters, including concentrations of the polyols ethylene glycol, glycerol, and erythritol, affected the size of synthesised vaterite nanoparticles. It was found that increasing concentrations of ethylene glycol and glycerol decreased the size of particles, as well as decreasing the rate of transformation of vaterite into other phases. However, erythritol was not studied as extensively as at the temperatures used (up to 40 °C) its solubility was too low to be used in high concentrations. The author of this dissertation therefore decided to use erythritol, as well as longer chained polyols, in higher

temperature systems where larger concentrations could be used.

## 2.2 Experimental Section


In reactions comparing the effect of different polyols on otherwise similar systems, the moles of alcohol groups was kept constant, i.e. a ratio of 3:2:1.5:1.2:1 mol of ethylene glycol:glycerol:erythritol:xylitol:sorbitol was used (where the number of alcohol groups in each molecule is 2:3:4:5:6). This results in a weight difference of less than 3% between the amount of polyol used, and a non-noticeable difference in volume. This was done as it has been postulated that hydroxyl groups act as nucleation sites for crystal growth, and therefore by keeping the number of hydroxyl groups same this effect is screen out, allowing for other effects of polyols to be elucidated.<sup>49</sup> In the methodologies shown below the masses for reactions with glycerol are used.

In reactions comparing the effect of different amounts of the same polyol, the same total volume of polyol and water was used throughout.

### *CaCO<sub>3</sub> synthesis via direct precipitation*


In a typical reaction 3.08 g CaCl<sub>2</sub> was dissolved in 10 ml deionized water in a round bottom flask before 100 g glycerol was added. The flask was sealed and placed to stir and heat in an oil bath set to 90 °C. In a separate flask 3.2362 g Na<sub>2</sub>CO<sub>3</sub> was dissolved in 40 ml deionized water before 70.4 g glycerol was added, afterwards which the vessel was sealed and placed to heat in an oil bath set to 90 °C. Once both vessels had reached temperature the Na<sub>2</sub>CO<sub>3</sub> solution was added to the flask containing the CaCl<sub>2</sub> solution before it was sealed again. White precipitate formed immediately upon mixing. The reaction was allowed to proceed for 30 minutes.

After reaction, the mixture was ‘cleaned’ by being centrifuged and redispersed with ethanol



two times, then centrifuged and dispersed in hot deionized water once, then centrifuged and redispersed in ethanol once, before finally being centrifuged and dried in a vacuum oven. (For reactions using erythritol the first centrifugation/redispersion cycle uses hot water, and the following three use ethanol).

For experiments where reaction times were under 30 minutes a different method for ‘cleaning’ was used in order to halt the reaction whilst the solid was isolated. Whilst setting up the



reaction glass syringes with metal needles were placed to heat in a convection oven set to 100°C. Hot syringes were used to extract samples from the reaction vessel and then be added to a centrifuge tube filled with isopropyl alcohol. The centrifuge tube was then closed and rapidly shaken. Afterwards this was centrifuged and redispersed in ethanol three times before being dried in a vacuum oven.

### ***CaCO<sub>3</sub> synthesis via ureolysis***

In a typical reaction (50 vol% glycerol) 0.83 g CaCl<sub>2</sub> was dissolved a vial containing 15 ml deionized water. The solution was allowed to cool to room temperature before 1.35 g urea was dissolved in it, afterwards which 18.9 g glycerol was added, the vial was sealed and shaken to mix the contents. The vial was then placed in a convection oven set to 90 °C and left overnight to react. The contents were filtered under vacuum and washed with ethanol and hot deionized water before being dried in a vacuum oven.

### ***CaCO<sub>3</sub> synthesis via vapour diffusion***

In a typical reaction 1.97 g CaCl<sub>2</sub> was dissolved in a vial containing 14 ml deionized water before 6.816 g glycerol was added and mixed. The vial was left open and sealed inside a desiccator containing 30 g ammonium carbonate in a separate open vial. The desiccator was placed inside a convection oven set to 30 °C and the reaction was allowed to proceed for 24 hours. The contents were filtered under vacuum and washed with ethanol and hot deionized water before being dried in a vacuum oven.

## 2.3 Results and Discussion

The synthesis of calcium carbonate was carried out in various conditions. Linear polyols ethylene glycol (EG), glycerol, erythritol, xylitol, and sorbitol were used as growth modifiers in aqueous reactions to form crystals of various morphologies and polymorphs.

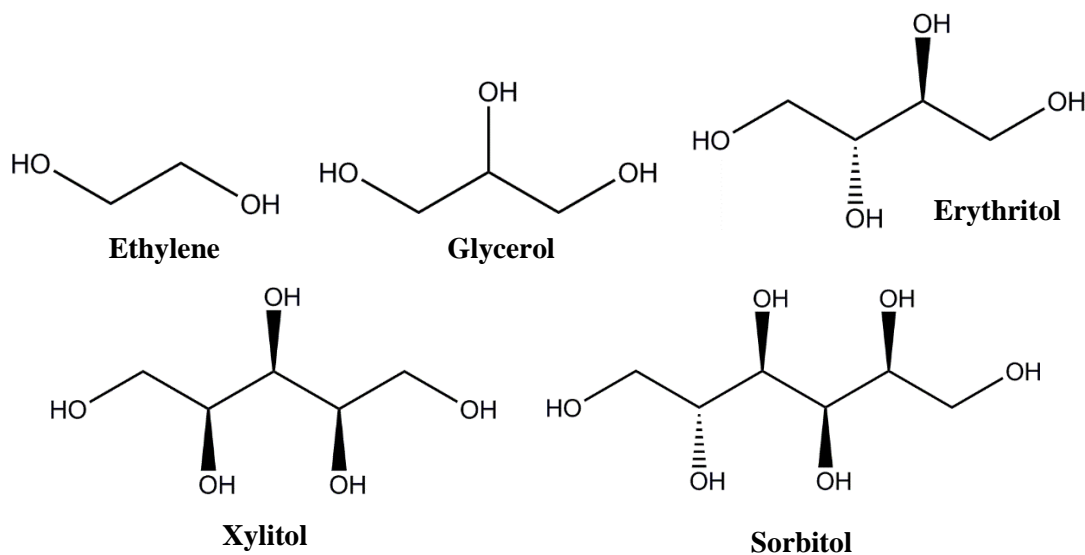


*Figure 1 – Chemical structures of used linear polyols.*

### 2.3.1 Effect of polyol length on morphology of $\text{CaCO}_3$

Calcium carbonate particles formed by direct precipitation at 90 °C produced different morphologies of the vaterite polymorph when different polyols were used, as shown in Figure2.

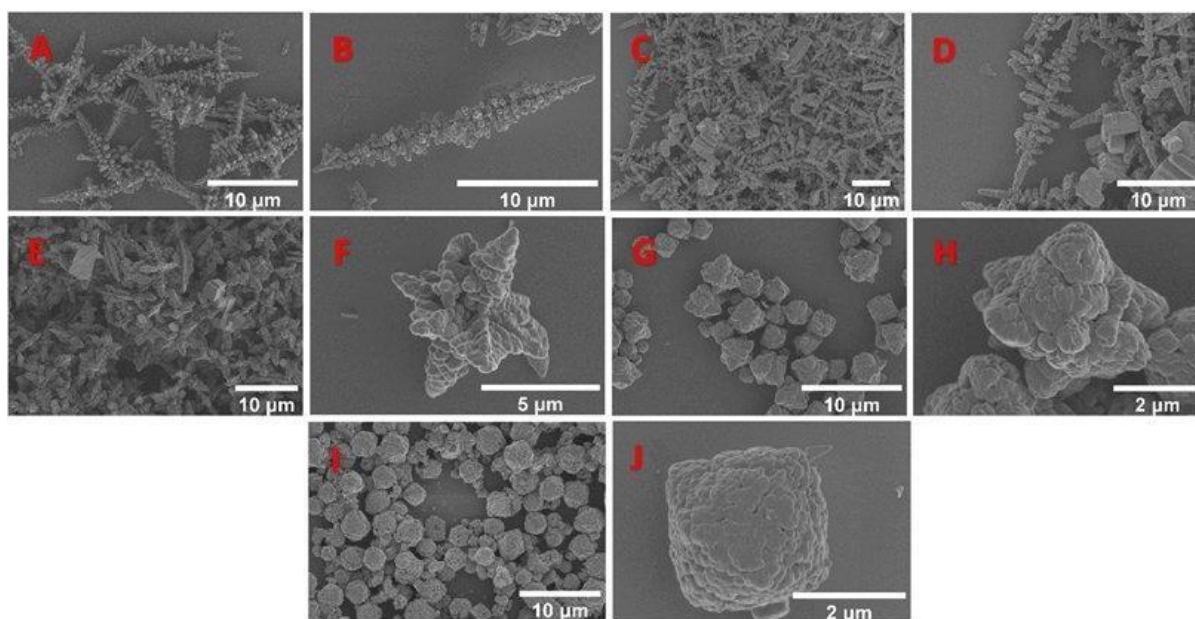


**Figure 2 – SEM micrographs of  $\text{CaCO}_3$  particles formed from solutions containing different polyols. (A,B) Ethylene glycol. (C,D) Glycerol. (E,F) Erythritol. (G,H) Xylitol. (I,J) Sorbitol.**

Particle size decreases with increasing polyol length, which has been observed before in polyol systems.<sup>49</sup> As in these experimental conditions the amount of hydroxyl groups from polyol molecules has been kept constant, this cannot be attributed to a higher number of nucleation sites causing more (and smaller) particles to be formed based on number of hydroxyl groups alone. It is possible however that an increase in polyol chain length causes a lower solubility (and therefore higher supersaturation) of calcium carbonate, thereby increasing the rate of nucleation and forming smaller particles.

Another notable feature is that there seems to be a morphological transition as polyol length increases, from long loosely packed globules around a central rod to a much more compact shape. Throughout this transition there seems to be wider masses towards the center of the rod, and these exhibit a hexagonal motif, two traits which are characteristic of vaterite. Spherulitic (fractal) growth is commonly seen in vaterite, and helps explain why the particles are wider in the centre of the of longest axis.<sup>21,40,43</sup> It is also interesting to note that very similar morphologies have been found in the literature from experiments with different reaction conditions, shown in Figure 3.<sup>44,50</sup>

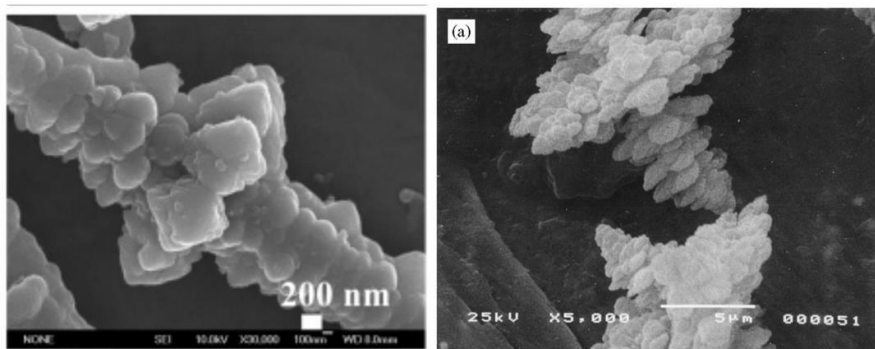


**Figure 3 – SEM micrographs of  $\text{CaCO}_3$  particles found in literature. (Left) from reference 40. (Right) from reference 46. DECLARATION: These images are not connected in any way with this author.**

The image on the left in Figure 3 is a vaterite particle formed in an ethylene glycol system which used SDS as a surfactant. The authors proposed that the shape was due to agglomerates of nanosized vaterite particles being stabilised by SDS assembling. However, the proposed mechanism of nano-aggregation (as opposed to classical crystal growth) has been discredited by a study by Andreassen.<sup>42</sup> Additionally the appearance of this morphology, in this dissertation and elsewhere in the literature, suggests that the proposed mechanism using SDS is incorrect. The image on the right in Figure was produced in a 10 vol% solution of ethanol, and similarly shows many comparable features to particles made from the high temperature polyol system.

One possible explanation for the morphological transition shown between polyol lengths is if specific faces of the growing crystal are poisoned by the adsorption of alcohol groups on the polyol. If the alcohol groups of the polyols prefer to adsorb onto a specific face, that face will experience retarded growth. Longer polyols may exhibit a chelating effect, whereby the multiple alcohol groups attached to the same alkyl chain causes an increase in the time which alcohol groups adhere to a specific face, thereby exaggerating the poisoning effect on this face. As a result this could explain how as the polyol chain length increases the particle morphology goes from a long dagger-like (a term coined by the authors from reference 40) rod to a more truncated, but similar, morphology. This explanation however lacks supporting data.



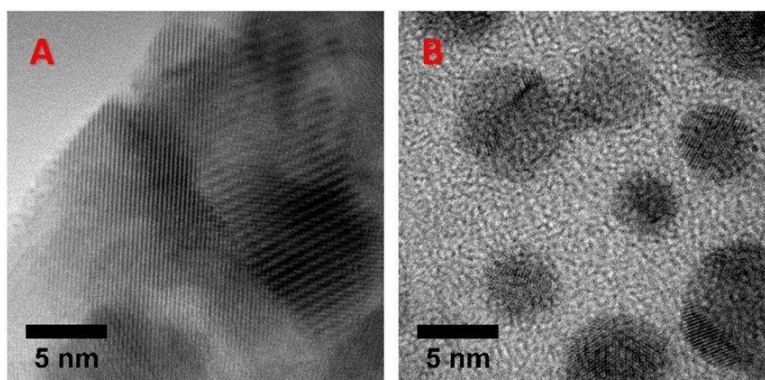


**Figure 4 – TEM micrographs of  $\text{CaCO}_3$  synthesised with glycerol. (Left) edge of a dagger-rod. (Right) crystals not attached to a larger object.**


TEM images of the sample produced in a glycerol solution (Figure 4) reveal the polycrystalline nature of these vaterite particles, as has been shown with other vaterite particles in literature.

### 2.3.2 Effect of reaction time on $\text{CaCO}_3$ particle morphology

The reactions in the ethylene glycol and glycerol systems were sampled at different times, shown in figure 5.

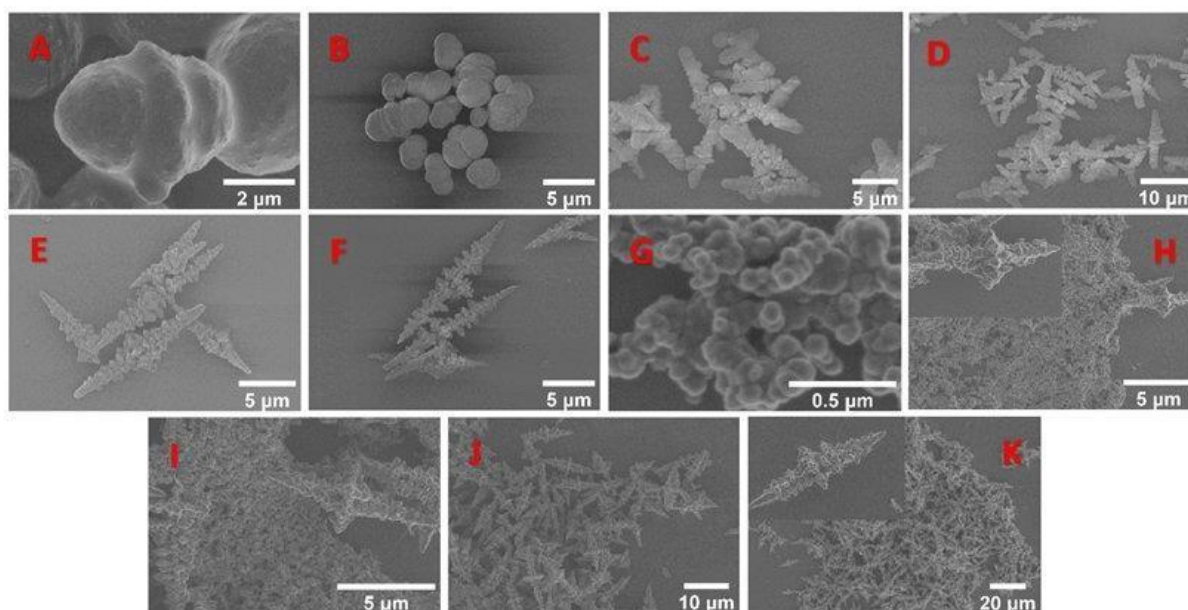


**Figure 5 – SEM micrographs of  $\text{CaCO}_3$  particles at different reaction times. (A-F) Ethylene glycol, times 10 sec, 30 sec, 1 min, 3 min, 5 min, 30 min. (G-K) Glycerol, times 10 sec, 1 min, 3 min, 5 min, 30 min.**



Looking at the ethylene glycol system at 10 and 30 seconds it can be seen that whilst the particles are much smaller, they exhibit a similar morphology in that there is a central wider region. As the reaction progresses the length of the particles increases and the rougher surface appears, and at 5 minutes the morphology appears to be very similar to that at 30 minutes. This seems to support the spherulitic growth mechanism of these particles which was previously mentioned.

For the glycerol system the same trend is not seen. At 10 seconds agglomerations of nanosized masses dominate. At one minute there appears to be a combination of the same small masses as well as very small amounts of ‘fully sized’ dagger-rods. At 3 minutes there is also a combination of small masses, along with a higher amount of fully sized particles. Similar to the ethylene glycol system, at 5 minutes the reaction seems to only contain fully formed particles, and there is little difference compared to the system at 30 minutes.

It was expected that a similar growth mechanism would be seen in these two systems. There is however too little data to surmise whether this difference is due to an actual difference in growth mechanism or if experimental error is to blame. As these systems change rapidly in the early seconds of reaction, small differences in how samples were taken can result in large difference. For example, improper mixing of the aliquoted sample that is injected into IPA to arrest growth could result in particle growth continuing. It is also possible that the difference in solubility of ethylene glycol and glycerol in IPA could have an effect on how quickly particle growth is arrested.

### 2.3.3 Effect of temperature on $\text{CaCO}_3$ particle morphology

The same direct precipitation conditions as shown previously were examined at lower temperatures for the ethylene glycol and glycerol systems (the longer chained polyols were not soluble at these temperatures in the same concentration).

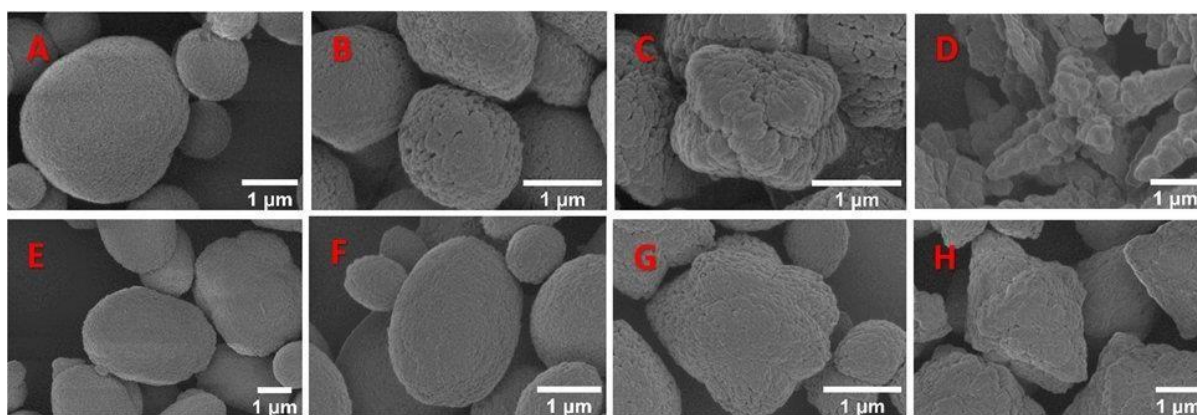


**Figure 6– SEM micrographs of  $\text{CaCO}_3$  particles produced at different temperatures. (A-D) Ethylene glycol. (E-H) Glycerol. 30, 45, 60, 75 °C from left to right.**

At the lower temperatures, 30 and 45 °C, elongated spherical particles were observed. At the higher temperatures, 60 and 75 °C, the morphology for both the ethylene glycol and glycerol systems seemed to shift towards those observed previously.

### 2.3.4 Effect of glycerol concentration on $\text{CaCO}_3$ particle morphology

Previously a 73 vol% of glycerol was used in the synthesis. Figure 7 shows reactions carried out over a range of range of different glycerol vol%.

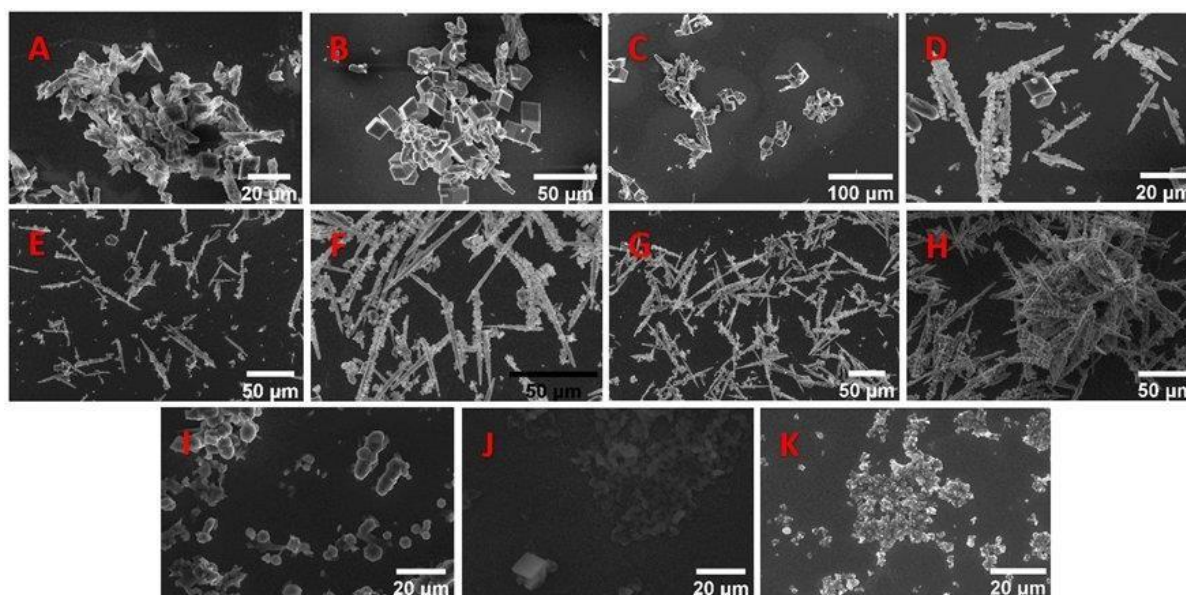


**Figure 7 – SEM micrographs of  $\text{CaCO}_3$  particles synthesised at various glycerol concentrations. (A-K) 0, 10, 20, 30, 40, 50, 60, 70, 80, 90, 95 vol%.**

At lower glycerol concentrations, 0-20 vol%, there are particles of rhombohedral calcite, as well as what is believed to be spindle-like vaterite particles. At 30 and 40 vol% dagger-rods appear, with calcite cubes still present. Between 50 and 70 vol% there only appear to be dagger-rods. At higher concentrations smaller and more rounded shapes are present, without any dagger-rods being visible.

The disappearance of calcite with increasing glycerol concentration agrees with studies in the literature that show transformation of other phases to calcite being suppressed with higher concentrations of alcohol moieties in solution. At the concentrations 80 vol% and above the reaction mixture became very viscous on the onset of crystallization, to the point that it appeared to not be stirring at all. This, along with other factors caused by increased glycerol concentration such as a higher supersaturation could be causing the drastic change in particle morphology. This change is poorly understood and can not be commented on more without further investigation.

### 2.3.5 $\text{CaCO}_3$ synthesised via vapour diffusion

Calcium carbonate was synthesised using a vapour diffusion method with various polyol and methanol containing solutions. Due to this being done at a lower temperature (30 °C) lower concentrations of polyols were used (roughly 15% of the amount used in previous systems).

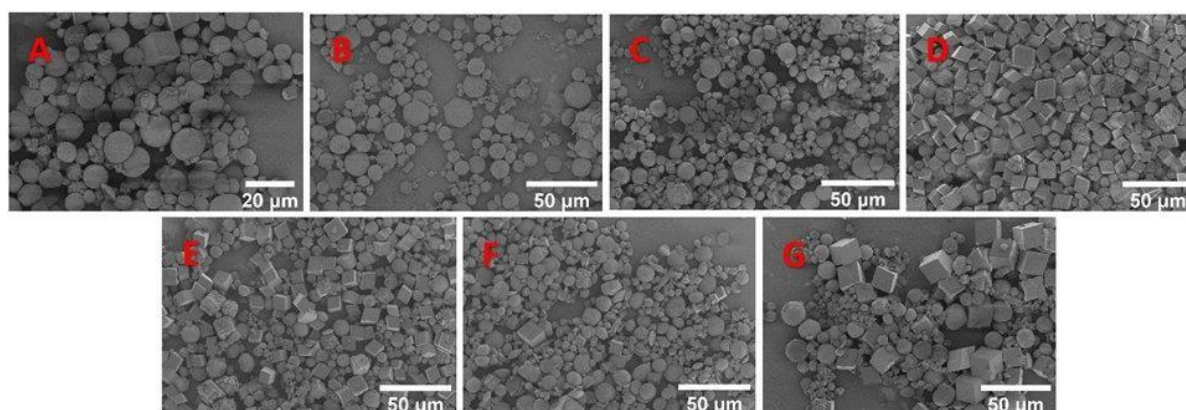


**Figure 8 –  $\text{CaCO}_3$  synthesised via vapour diffusion. (A) ethylene glycol. (B) glycerol. (C) erythritol. (D) xylitol. (E) sorbitol. (F) water only. (G) methanol.**

Visually all these systems seem similar, containing a combination of vaterite spheres/hexagonal shapes as well as calcite cubes. It is possible that there is a difference in polymorphic abundances between the samples, but without further data (for example from XRD measurements) this is currently not possible to comment on. It is also possible that at these lower concentrations of alcohols the effect they exert on the growth of calcium carbonate crystals is minimal.

### 2.3.6 Effect of glycerol concentration on $\text{CaCO}_3$ formed by ureolysis

Calcium carbonate particles were synthesised via ureolysis reactions in solutions containing varying vol% of glycerol.



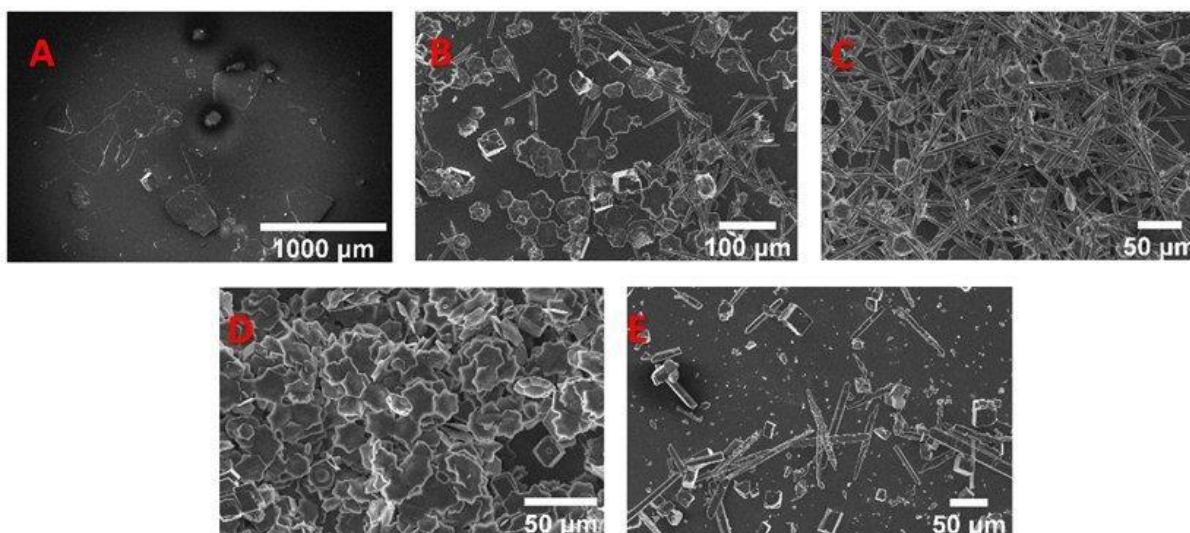



**Figure 9 - SEM micrographs of  $\text{CaCO}_3$  particles formed by ureolysis in solutions with varying glycerol vol %. (A) 0 vol%. (B) 25 vol%. (C) 50 vol%. (D) 75 vol%. (E) 95 vol%.**

In the pure water reaction large flakes, some visible to the naked eye, and smaller cubes were formed, assumed to be calcite. At 25 vol% there was a mixture of calcite cubes, rod shaped aragonite, and hexagonal flower shaped vaterite. At 50 vol% there were mainly rods, with some flowers, and few cubes. At 75% flowers seem to be the dominant morphology, with some cubes also being present. At 95 vol% there are rods and cubes present, with no evidence of vaterite flowers. The increase in glycerol concentration initially seeming to reduce the amount of calcite present agrees with previous reports of polyols suppressing the transformation of less stable polymorphs to calcite. The 95 vol% reaction however does not follow this trend.

## 2.4 Conclusions

Polyols have been shown to affect the morphology as well as polymorphic abundance of synthesised calcium carbonate particles. These effects seem to be more pronounced at higher concentrations of polyol as well as higher temperatures. It was found that there was a significant increase in abundance of non-calcite polymorph particles due to the use of polyols. Dagger-like morphologies were found to be produced, with a trend showing higher aspect-



ratio particles when shorter chained polyols were used, and lower aspect-ratio particles when longer chained polyols were used.

It is not certain what the reason for the shown effects are, but it is possibly due to change in solubilities (and therefore solution supersaturation) of calcium carbonate in the different reaction compositions. The viscosity differences between the different polyol solutions could also be a factor affecting the outcome of these reactions.

In chapter 3 some of the calcium carbonate particles produced were used as templates for the synthesis of hybrid microparticles. In chapter 4 some of these particles were tested for their ability to clean teeth in toothpaste formulations.



## **CHAPTER 3**

### **“Calcium carbonate particles as templates for synthesis of hybrid microparticles”**

In this chapter calcium carbonate particles are coated in silica and polymer materials. Calcium carbonate particles are used as sacrificial templates to produce calcium fluoride particles of similar morphologies.



### 3.1 Introduction

Calcium carbonate particles produced in chapter 2, as well as samples obtained from commercial suppliers, were used as templates for further reactions, creating hybrid microparticles. Seeded dispersion polymerization reactions allowed for the polymer coating of calcium carbonate particles. The additional removal of the calcium carbonate core formed hollow polymer particles, which were to be tested for their ability to release a oil-based payload. Coating of calcium carbonate particles with silica was desired for an increased hardness of the particle surface, with the hope of increasing the abrasive cleaning ability.

Finally particles were used as a sacrificial template for the production of calcium fluoride particles of the same morphology as the template.

### 3.2 Experimental Section

#### *Polymer coating of calcium carbonate particles ( $\text{polymer}@CaCO_3$ )*

In a typical reaction 300 mg of monomer, 900 mg calcium carbonate particles, and 10 mg AIBN are added to a vial containing 15 ml acetonitrile. The vial is sealed and degassed with nitrogen for 10 minutes before being rotated in a heated oven at 25 RPM. The reaction mixture is heated from room temperature to 70°C over an hour before being left at temperature for 5 hours to allow for polymerization. The mixture is then allowed to cool to room temperature before being centrifuged and redispersed in acetone three times. The particles are then dried in a vacuum oven.

#### *Calcium carbonate to calcium fluoride conversion ( $CaF_2@CaCO_3$ )*

In a typical reaction (with 100% theoretical conversion) 0.2098 g sodium fluoride is dissolved in 25 ml of deionized water. While the solution is being stirred 0.25 g of calcium carbonate is added to the solution and allowed to react. The mixture is then filtered and washed with deionized water before being dried in a vacuum oven.

### ***Silica coating of calcium carbonate particles ( $\text{SiO}_2\text{@CaCO}_3$ )***

In a typical reaction 8 g calcium carbonate, 8 ml deionized water, and 72 ml ethanol are added to a round bottom flask and stirred. 4 ml 35 vol% ammonia is added and allowed to stir for 10 minutes. 0.8 g tetraethyl orthosilicate (TEOS) is added at a rate of  $0.13 \text{ g hr}^{-1}$  with a syringe pump, and then allowed to react for a further 6 hours or more to form  $\text{SiO}_2$ . The contents are then centrifuged and redispersed in a 1:1 solution of water:ethanol three times before being dried in a vacuum oven.

### ***Formation of magnetite on acid functionalised hollow polymer shell***

In a typical reaction 0.1 g acid functionalised polymer particles was added to 50 ml deionized water and the pH adjusted to 6.3 with 0.5 M potassium hydroxide solution before the vessel was sealed, stirred, and purged with nitrogen for 15 minutes. 0.305 g potassium sulphate heptahydrate was dissolved in 5 ml deionized water before being flushed with nitrogen for 5 minutes and then added to the main vessel. The vessel was then flushed with nitrogen for a further 10 minutes before being put under overpressure of nitrogen and allowed to stir overnight. The contents of the vessel were dialysed in a cellulose membrane against deionized and nitrogen purged water for 2 hours. The dialysed mixture was then stirred in a round bottom flask under nitrogen pressure. 0.182 g sodium nitrite was dissolved in 5 ml deionized water and purged with nitrogen for 10 minutes before being added to the polymer containing flask. Finally 17.5 ml 35% ammonia solution was added to the flask and allowed to stir for 1 hour, forming a black precipitate. The contents were then centrifuged and redispersed deionised water three times before being dried in a vacuum oven.

In a typical reaction 1 g of material is dispersed and stirred in 10 ml of deionized water. 40 ml of 0.5 M acetic acid is added over 2 hours with a syringe pump, and then allowed to stir for another hour. The contents are then centrifuged and redispersed in deionized water three times before being dried in a vacuum oven.

### 3.3 Results and Discussion

#### 3.3.1 Polymer coating of $\text{CaCO}_3$ particles

The synthesis of polymer coated calcium carbonate particles was adapted from a procedure previously reported by Bon and Ballard.<sup>51</sup> It proceeds via a free radical precipitation polymerization mechanism shown in the figure below.

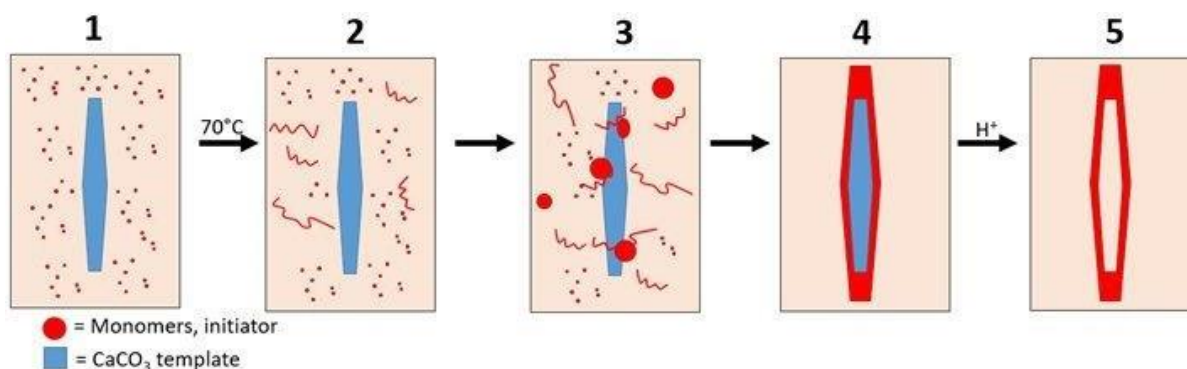


*Figure 10 - Schematic of polymer coating of  $\text{CaCO}_3$  particle template*

Referring to Figure 10, in stage (1) calcium carbonate particles, monomer, and initiator are added to a solvent. This system uses acetonitrile as a solvent and the initiator, azobisisobutyronitrile (AIBN), as well as the monomers used, methacrylic acid (MAA), acrylic acid (AA), and divinylbenzene (DVB) are fully soluble at the used concentrations. Commercially available precipitated calcium carbonate rods of the aragonite polymorph ‘Whiscal A’ are used as templates in this system. In stage (2) the reaction is agitated (in this system by having the vessel rotated in a heated oven) and heated to 70 °C so the AIBN decomposes, forms radicals, and initiates the polymerization. After a certain chain length has

been achieved polymers will no longer be soluble and crash out of the solution, either forming free latex particles or sticking to the calcium carbonate particle surface, shown in stage (3). As the reaction proceeds monomer will eventually be used up, resulting in a mixture of hybrid polymer coated calcium carbonate particles and free polymer latex, shown in stage (4). If desired the calcium carbonate core can be removed by dissolution with an acidic solution (etched), resulting in a hollow polymer shell, shown in stage (5).

Various compositions of monomer were used to coat the calcium carbonate particles, shown in Figure X.

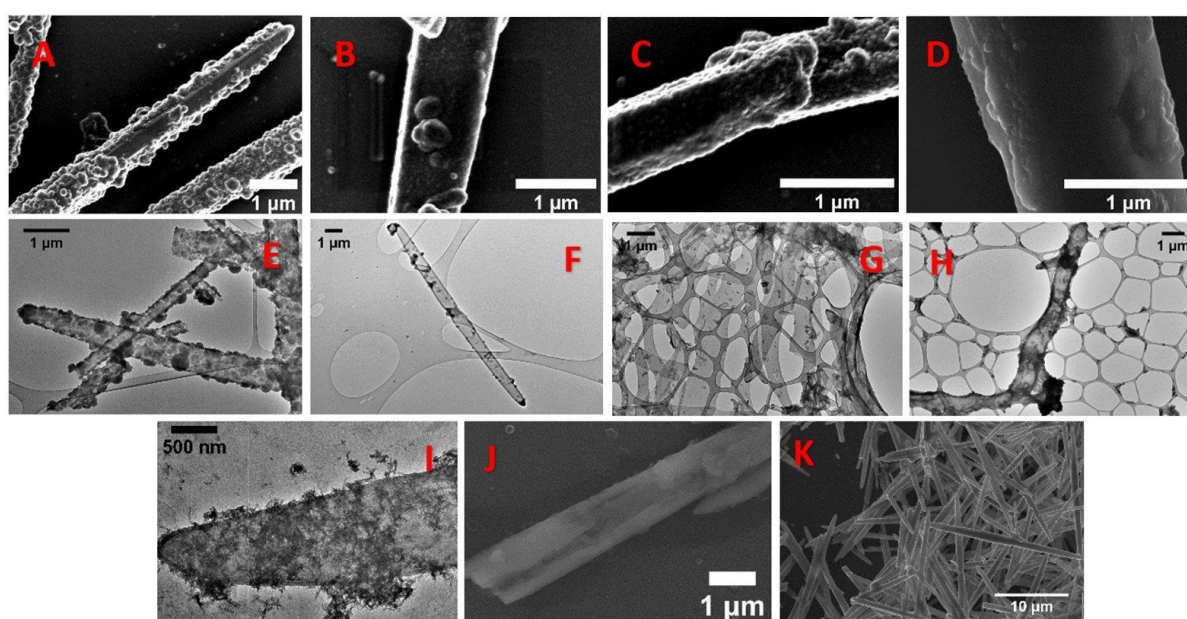


**Figure 11 - Micrographs of polymer coated and etched hollow polymer shells of different monomer compositions. (A,E) 100% DVB. (B,F) 50% DVB 50% AA. (C,G) 10% DVB 90% AA. (D,H,I) 100% AA. (J) 10% DVB 90% MAA. (K) Whiscal A  $\text{CaCO}_3$  rod used as the template for all coatings.**

When only the crosslinking monomer DVB was used particles were not fully covered and high amounts of free latex was present in the supernatant of the centrifuged product. With this composition the instability of larger latex particles, as well as the collision between latex and calcium carbonate particles are the driving factors resulting in polymer adherence to calcium carbonate template. Additionally, when the template does have polymer on it, the coating is uneven and looks like it is covered by varying sizes of latex spheres. When 50%, 90% and

100% of the monomer (by weight) is acrylic acid, the template appears to be fully covered with a much smoother finish. This is likely due to the interaction the carboxylate group of the acidic monomer has with surface calcium atoms of the calcium carbonate crystal. What can also be observed in the TEM micrographs (G,H,I) is that when 90% and 100% acrylic acid is used the hollow etched polymer shell deforms from the original straight shape of the template, which could be due to the lower crosslinking density in these compositions giving them higher flexure. In image I the shell itself seems to be falling apart due to the lack of crosslinking. When 90% MAA was used (Image J), shells were often cracked after etching, possibly due to the materials lower flexibility causing ruptures as carbon dioxide bubbles formed within the shell during calcium carbonate dissolution.

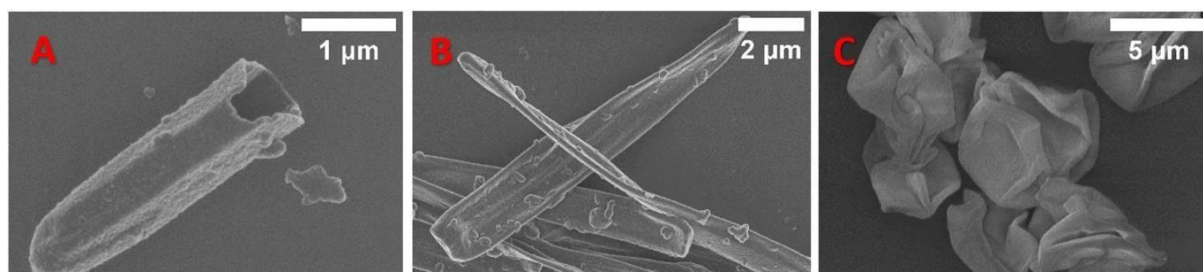


**Figure 12 - SEM micrographs of hollow polymer shells. (A) broken rod shell. (B) unbroken rod shell. (C) unbroken spherical shell.**

Figure 12 shows the effect the vacuum conditions of the electron microscope has on the morphology of the hollow polymer shells. In image A the broken shell retains the hexagonal structure of the template particle, whilst in images B and C the structures seem to have collapsed on themselves, which could be due to the air (or liquid) trapped inside the shell causing negative pressure as it is pulled out during vacuum. It is not known whether these shells would regain their original shape over time or with the introduction of a solvent, or if they have become permanently deformed.

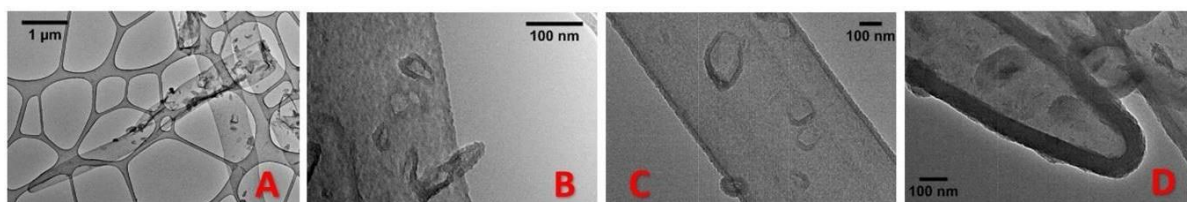


**Figure 13 - TEM micrographs of etched polymer shells of varying thickness. (A) 1 wt% monomer wrt  $\text{CaCO}_3$  template. (B) 5 wt%. (C) 10 wt%. (D) 20 wt%.**

Figure 13 shows hollow polymer shells of 1:1 AA:DVB which were synthesised at different wt% of monomer with respect to mass of the calcium carbonate template. From these images wall thicknesses were measured to be 8, 25, and 50 nm for the 5, 10, and 20 wt% systems, whilst for the 1 wt% shell there was not enough contrast to deduce a thickness. These measurements are however prone to error as they are simply based on image contrast on the edge of the particles, and without knowing if/how the shells are deformed (as seen in Figure 12) it is not known if this image contrast relates a folded shell or not (which would imply the measured thickness is roughly double of the actual thickness).

Overall, the aim of coating calcium carbonate templates with a polymer shell, as well as producing hollow polymer shells, was successful.

### **3.3.2 Silica coating of $\text{CaCO}_3$ particles**

The synthesis of silica coated calcium carbonate particles was adapted from previous work within the research group, which is based on a templated version of the Stober synthesis of silica spheres.<sup>48</sup> Briefly, calcium carbonate is dispersed in a solution of water, ethanol, and ammonium hydroxide, to which tetraethyl orthosilicate (TEOS) is fed into over the course of hours. TEOS undergoes hydrolysis to form a silica network,  $\text{SiO}_2$ , which encapsulates the calcium carbonate template.



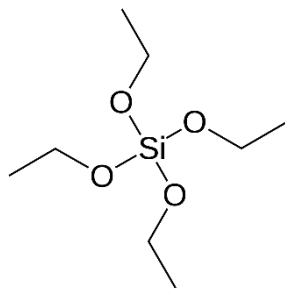


*Figure 14 – Structure of TEOS*

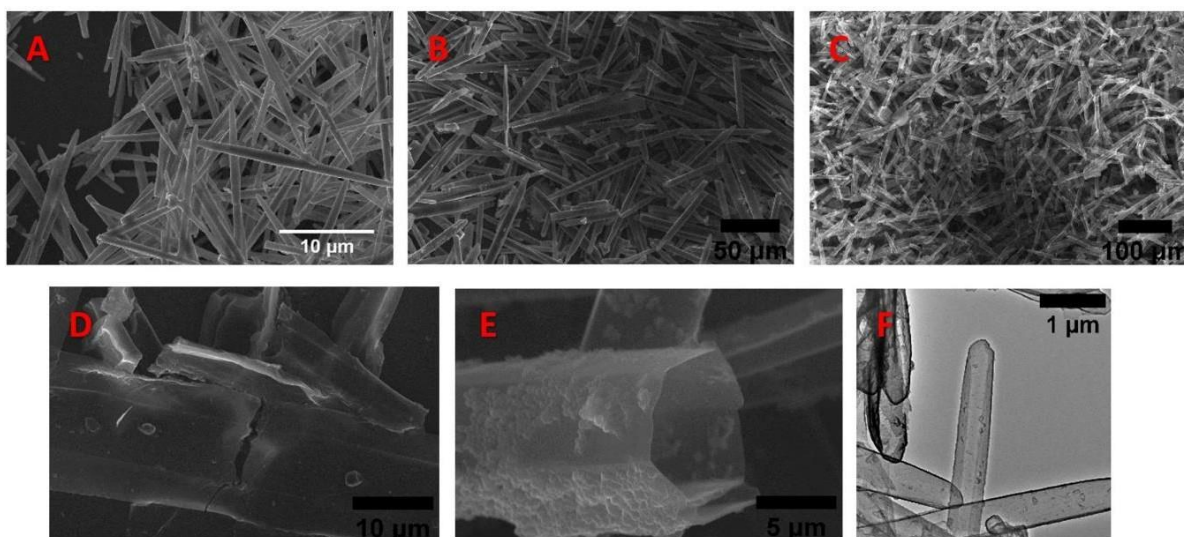


*Figure 15 – Micrographs of silica covered  $\text{CaCO}_3$  with different feed rates of TEOS. (A) Whiscal A  $\text{CaCO}_3$  template. (B,D,F) TEOS feed  $0.13 \text{ g hr}^{-1}$ . (C,E) TEOS feed  $0.26 \text{ g hr}^{-1}$*

Figure 15 shows the effect that feed rate of TEOS had on particle morphology. When a feed rate of  $0.26 \text{ g hr}^{-1}$  was used (image E, showing the silica shell after the calcium carbonate had been removed via acid etching) there were spheres on the outside of the hollow shell, whereas when a rate of  $0.13 \text{ g hr}^{-1}$  was used (image D) the shells were smooth. This is most likely due to the higher rate resulting in higher secondary particle nucleation which formed silica spheres (as with the traditional Stober synthesis), instead of the added TEOS adding onto the silica network already formed on the template surface.

It was found that when this same experimental procedure was used for calcium carbonate particles of the vaterite polymorph (as opposed to the previously shown aragonite Whiscal A rods) that high amounts of coagulum was formed. It was hypothesised that this was due to the

vaterite particles recrystallising into calcite during the reaction whilst they were being coated in silica which could lead to large agglomerates of particles.

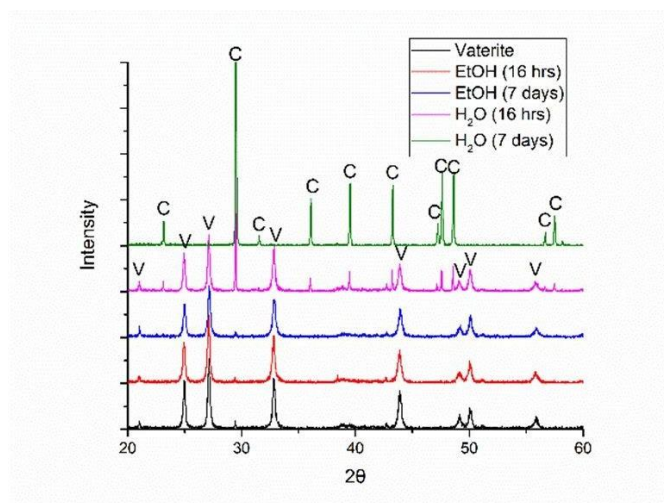


**Figure 16 – XRD Spectra of vaterite particles ages in ethanol and water.**

XRD spectra of vaterite particles which were submerged in ethanol and water for 16 hours, and for 7 days, were taken to see how stable this polymorph was in each solvent, which can be seen in Figure 16. After 7 days in ethanol there appears to be no transformation of the vaterite phase, whilst after 16 hours in water calcite formation is shown, and after 7 days the only polymorph present is calcite. One critical mistake with this data is that the solutions were left unstirred and so the change in polymorph is most likely under-represented. Taking this into account, along with the total reaction time of the silica coating synthesis being around 12 hours, it is possible that the transformation of vaterite into calcite is responsible for the coagulum in the reaction.

The synthesis was changed so that the only water present was in the ammonium hydroxide solution used (the removed water was replaced with more ethanol). This resulted in coated vaterite particles with no coagulum in the reaction, which are shown in Figure X.



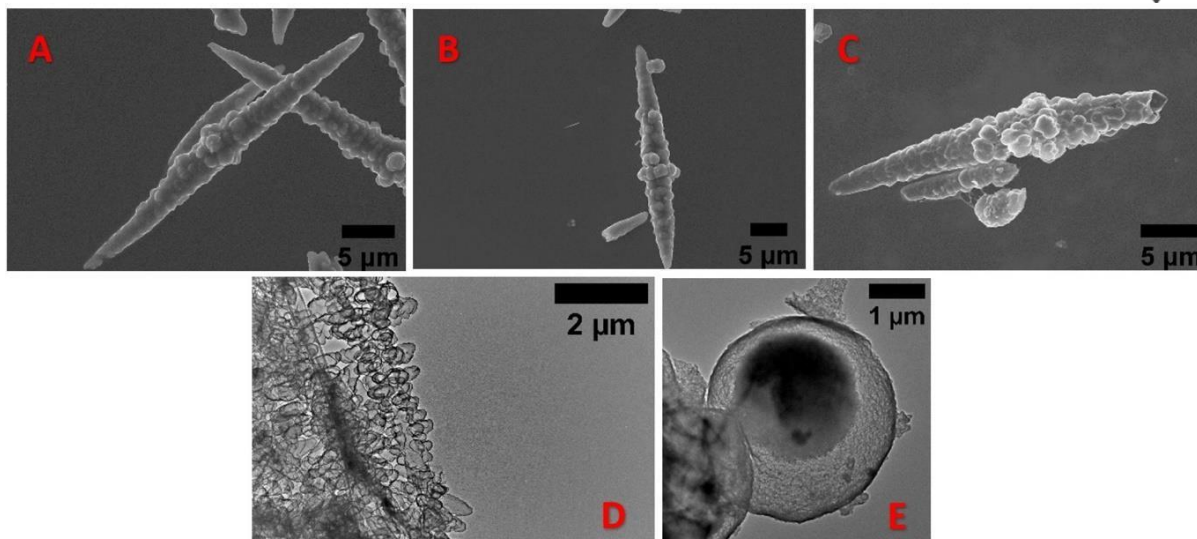


**Figure 17 – Micrographs of silica coated vaterite particles. (A) Vaterite used as template. (B) Silica coated vaterite. (C,D) Hollow etched silica particle. (E) Hollow etched silica sphere.**

Uniaxial compression tests of Whiscal A and silica coated counterparts were performed to examine the effect which the coating had on the particles strength, results of which can be seen in Figure 18.

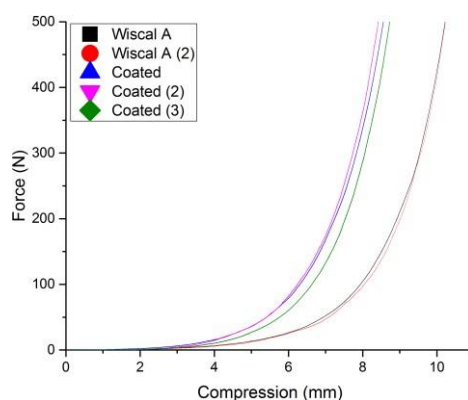


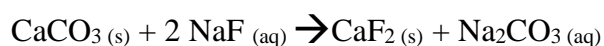
**Figure 18 – Uniaxial compression data of silica coated and uncoated Whiscal A particles**

The higher resistance to compression of the coated particles can be clearly seen as at any given force there is a lower compression of the coated particles. This is believed to be due to both the higher hardness of silica which makes the material more resistive to deformation, as well as its amorphous and less brittle nature relative to the crystalline calcium carbonate which

makes the needle like particles less likely to snap (which would cause fragmentation and allow further packing of the material).

### 3.3.3 Conversion of $\text{CaCO}_3$ particles to $\text{CaF}_2$

Synthesis of calcium fluoride particles was achieved by directly reacting dispersed calcium carbonate particles with aqueous sodium fluoride, driven by the lower solubility of calcium fluoride, as shown below.



As opposed to the previous polymer and silica coatings using calcium carbonate particles as templates, in this reaction the calcium carbonate is being used as a sacrificial template to create a new material with the aim of creating a particle of the same morphology.

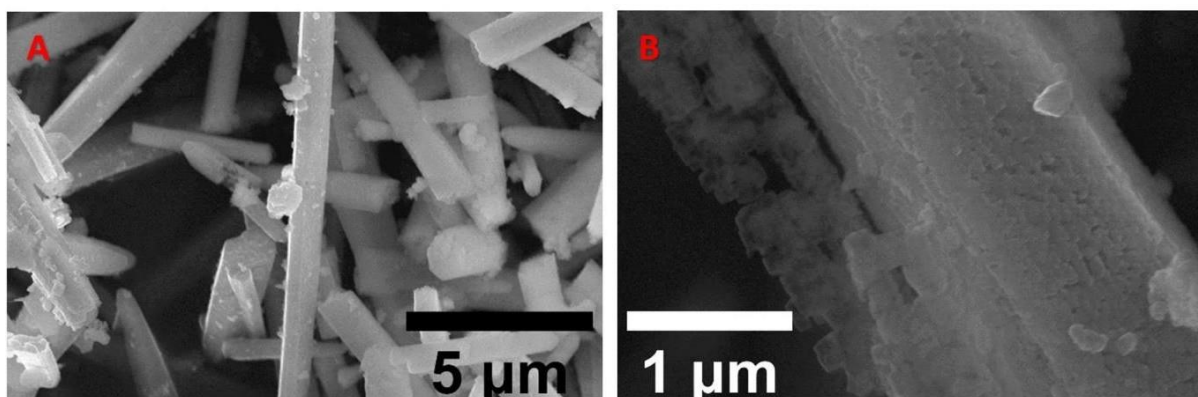


**Figure 19 – SEM micrographs of  $\text{CaF}_2$  particles from Whiscal A templates in a theoretical 100% conversion reaction.**

Figure 19 shows Whiscal A particles which have been reacted with a stoichiometric amount of sodium fluoride, yielding a theoretical 100% conversion. When a fluoride ion selective electrode (FISE) probe was used to measure the fluoride consumption as a function of time of a repeated experiment, it was found that even after 3 days of reacting nearly 25% of fluoride ions remained in solution. The solution pH at the start of reaction was 8.5, and after 3 days it

was 10.5, which can be attributed to the release of carbonate ions. At this point dilute acetic acid was added dropwise, which resulted in an almost instant reduction in the amount of measured free fluoride ions. This is shown in Figure 20.

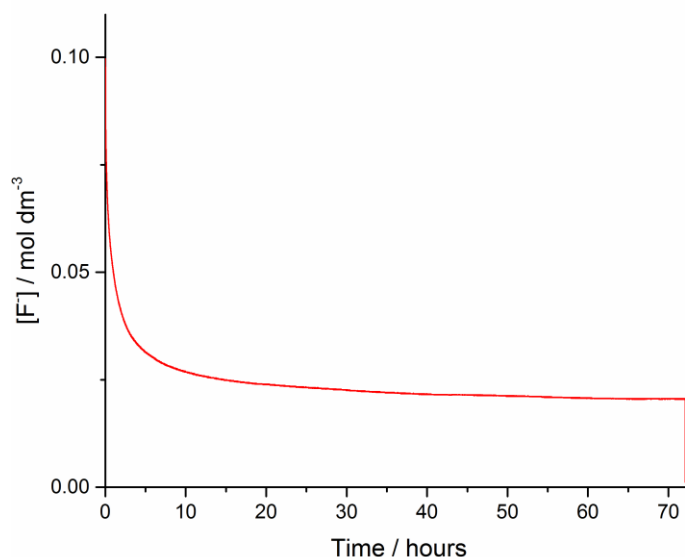


**Figure 20 – Free fluoride ion concentration measured over time.**

The increase in pH over the course of the reaction is assumed to lower the solubility of calcium carbonate, and therefore retard the surface precipitation reaction with free fluoride ions. Further experiments using an excess of sodium fluoride (500% of what is needed for the theoretical complete conversion) were performed to see if the complete conversion of calcium carbonate to calcium fluoride could be achieved without the need for acid addition. XRD spectra of these particles are shown in Figure 21.

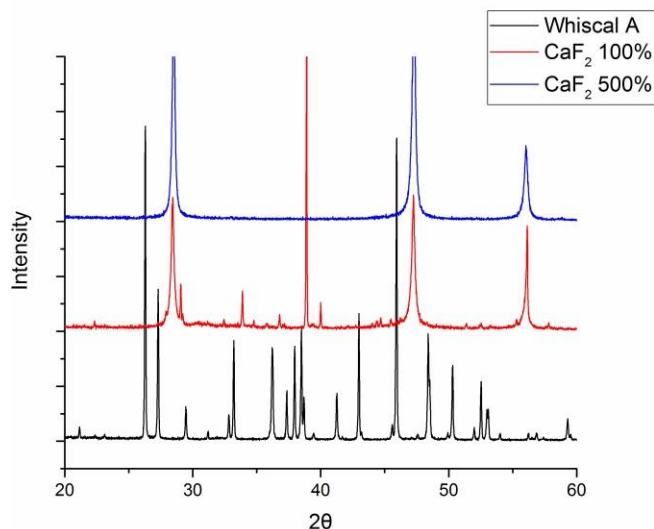


**Figure 21 – XRD spectra of  $\text{CaCO}_3$  template and  $\text{CaF}_2$  particles from a 100% and 500% conversion reaction.**

It can be seen that with the 100% conversion reactions that there was still calcium carbonate remaining in the sample, whereas the 500% reaction shows only calcium fluoride peaks. These particles, along with ones that were made with a 20% (deficient) stoichiometric amount of sodium fluoride, were etched with acetic acid, revealing differences in their internal structures, shown in Figure 22.

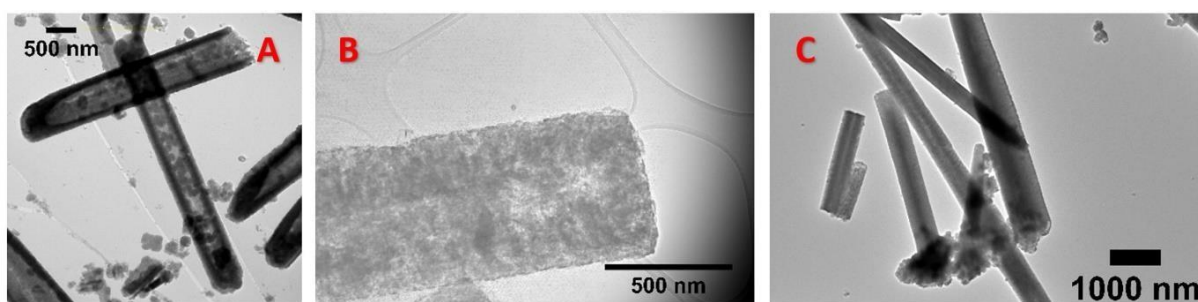


**Figure 22 – TEM micrographs of etched  $\text{CaF}_2$  particles. (A) 20% conversion. (B) 100% conversion. (C) 500% conversion**

The 20% converted particle have a large hollow core when the calcium carbonate has been removed by acid etching, showing how the reaction proceeds from the surface towards the inside of the particle. Both the 100% and 500% converted particles have voids running throughout the length of the particles, but the 500% seem to generally contain less voids.

Overall, the general morphology of the Whiscal A particles seem to translate to the final calcium fluoride particles, although there is a large amount of broken particle fragments. This lower structural integrity is expected due to the voids formed as a result of material volume shrinkage.

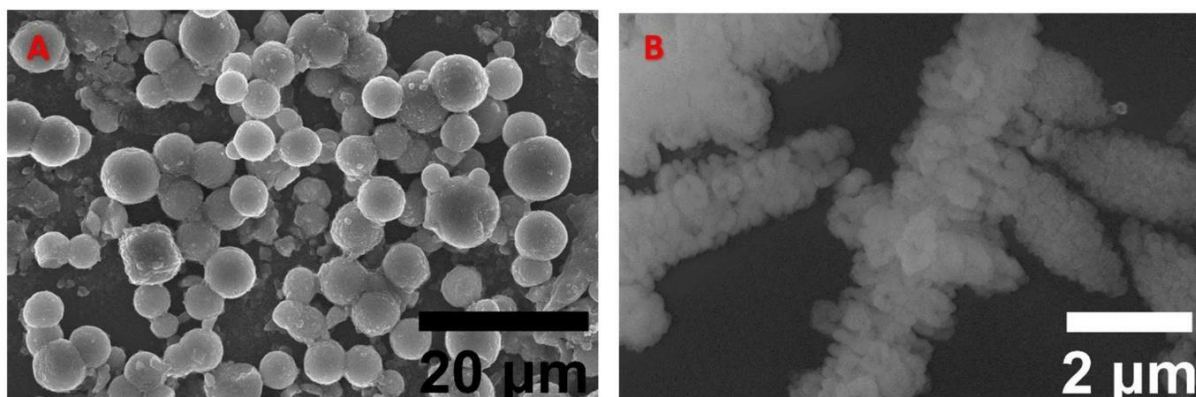


**Figure 23 – SEM micrographs of  $\text{CaF}_2$  particles from vaterite templates. (A) Spheres as templates. (B) dagger-rods as templates.**

Figure 23 shows other calcium carbonate morphologies being used as templates for the reaction. Like with the previously shown particles from Whiscal A templates, the general morphology seems to remain intact, but they have much coarser surfaces. The spheres show numerous pits on the surface, and the dagger-rods have had their particular surface morphology removed almost entirely, with only the general shape of a rod with a wider center still being present.

### ***3.3.4 Magnetite formation on acid-functionalised hollow polymer shells***

The synthesis of magnetite nanoparticles ( $\text{Fe}_3\text{O}_4$ ) particles attached to a template of acid-functionalised hollow polymer shells was achieved by adopting a procedure developed by Higashitani et al. where they fabricated p(styrene/NIPAM/MAA) latex particles containing magnetite.<sup>49</sup> Briefly, hollow polymer shells with acid functionalisation (shown previously in this chapter) were dispersed in water, iron ions were allowed to bind with the carboxylate

groups, and then the iron is oxidised to magnetite with hollow shell as the locus of the reaction.

A schematic of this procedure is shown in Figure 24.

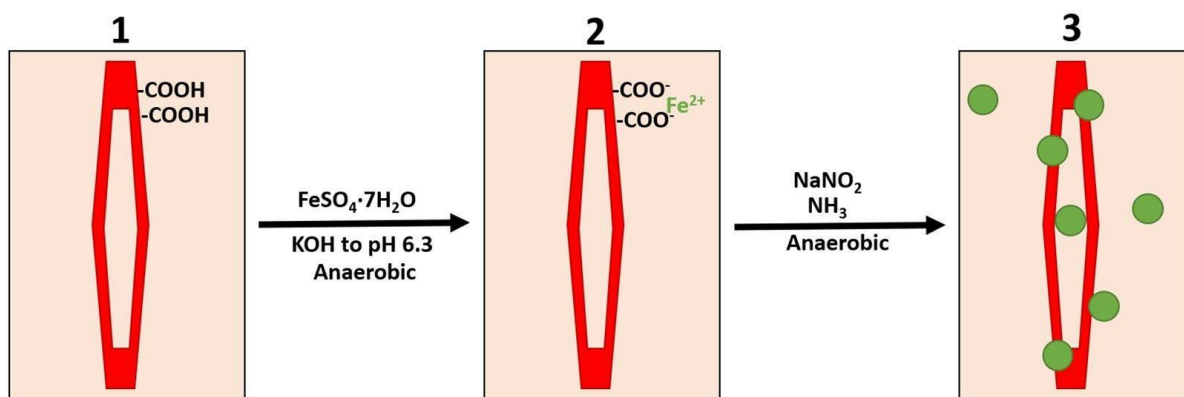


**Figure 24 – Schematic of magnetite formation with acid-functionalised hollow polymer shells as a template.**

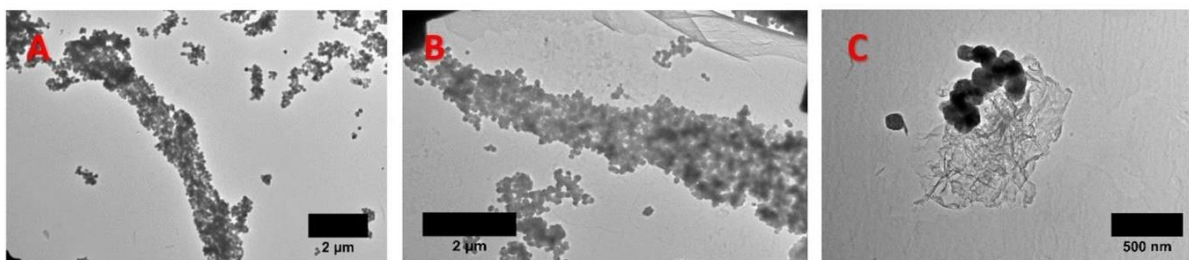



**Figure 25 – TEM micrographs of magnetite formed on hollow polymer shells.**

Whilst the magnetite seemed to show good coverage of the entire hollow polymer shells, there were large amounts of breakage of the polymeric material, shown in Figure 25.

### 3.4 Conclusions

Calcium carbonate particles were used as templates for further modification. Surface addition of polymeric and silica material allowed for the creation of hybrid core-shell particles, which when the calcium carbonate core was removed with acid etching formed hollow shell particles of solely the added material. Acid-functionalised hollow polymer shells were further used as a templates for magnetite functionalised hollow polymer shells,



although the structure of these particles was damaged significantly by the reaction. The use of calcium carbonate particles as sacrificial templates for the synthesis of calcium fluoride particles with the same morphology was also achieved.

Although the particles made showed that the syntheses worked, the produced particles had poor material properties. The polymer shells produced were often damaged, limiting their suitability for their desired role as particles to carry oil-based payloads.

Further work could be done to enhance the physical properties of the polymer shell whilst still producing particles with a high fidelity of copying the morphology of the template calcium carbonate particles.

Some silica coated particles produced were tested for their teeth cleaning ability in chapter 4.

---

## **CHAPTER 4**

### **“Testing cleaning ability of microparticles”**

In this chapter the dental cleaning ability of synthesised and commercially acquired calcium carbonate and silica particles are presented. The results are compared against a commercial standard product.



## 4.1 Introduction


With the desire of finding microparticles which had high tooth cleaning ability, various particles produced, which were shown in chapters 2 and 3, were tested for this using an industry standard method.

### 4.1.1 *Background to oral care*

Due to their constant exposure to the external world teeth are a location for the unwanted growth of microorganisms and precipitation of materials from saliva, food, and drink.<sup>54</sup> This can produce issues such as halitosis and unsightly teeth, or more seriously; periodontitis, caries, and infections, which can lead to tooth loss, atherosclerosis, and other cardiovascular diseases.<sup>55,56</sup>

Teeth are composed of several layers of different organic and inorganic materials. The harder two outer layers which provide their mechanical strength are the enamel and dentin. Hydroxyapatite,  $\text{Ca}_5(\text{PO}_4)_3(\text{OH})$ , is the mineral which makes up the majority of these materials by weight.<sup>57,58</sup> Enamel makes up the outer layer of teeth and is the harder of the two materials (5 on the Mohs hardness scale).<sup>59</sup> Dentin makes up the second layer of the tooth and is softer (3-4 Mohs hardness) due to its lower hydroxyapatite content and larger protein-containing amorphous regions.<sup>60</sup> Enamel contains no living cells and it is not repaired or replenished by the body when it is damaged. If enough enamel is removed from the surface of a tooth the underlying dentin is exposed. Although dentin can regrow, the process is slow and exposure to temperature gradients, mechanical force, and microbial can cause tremendous pain to its owner.<sup>61</sup> As the gumline in the mouth recedes over time to expose parts of teeth with a thinner layer of enamel, the cumulative issues and costs caused by tooth damage are proportionally higher in parts of the world which are faced with an aging demographic.<sup>62</sup>

Damage and removal of tooth material is caused both by physical mechanisms such chewing



and brushing, as well as the dissolution of hydroxyapatite from acids contained in food, drink, and the products from the breakdown of carbohydrates by oral microorganisms which grow of the tooth surface.<sup>63</sup> To protect the teeth glycoproteins contained in saliva bind to the tooth surface creating a protein film called dental pellicle.<sup>64</sup> This barrier acts to decrease degradation of the tooth surface by acid produced by microorganisms, as well as preventing mineral deposits forming on the tooth surface from compounds dissolved in saliva.

Certain microorganisms are attracted to these glycoproteins, attaching themselves to the pellicle layer, and forming a biofilm called plaque.<sup>65</sup> If this bacterial biofilm is not removed the protective effectiveness of the glycoproteins in the dental pellicle is reduced and minerals in saliva can precipitate onto the tooth surface. The precipitated minerals, as well as the organic material from dead microorganisms form a solid layer around the teeth called tartar. Initially only a limited number of microbes can thrive on the dental pellicle surface. Plaque and tartar provide a locus for the growth of additional types of microorganisms which previously could not survive in the tooth surface environment, accelerating the processes of bacterial growth and mineral precipitation, and the damage caused by these events. Constant cleaning of the teeth to remove plaque is required to prevent the formation of tartar and decrease the need for more intensive oral care.


#### ***4.1.2 Toothpaste design***

Dentifrices are powders, pastes, or liquids with the primary function of reducing these damaging events by removing plaque, tartar, mineral deposits, and food remains from the tooth surface.<sup>66</sup> A secondary function which is highly valued commercially is the removal of stains from the tooth surface which are caused by bound chromophores originating from ingested food and drink. The most widely used non-professional dentifrice products are toothpastes. In its simplest form toothpaste requires three components: an abrasive agent which mechanically removes debris, a thickening agent which suspends the abrasives in the formulation, and a

surfactant which aids in the removal of the debris.<sup>67</sup> In modern formulations abrasives make up a major portion of toothpastes (commonly 15-50 wt%).<sup>68</sup> Historically a wide range of materials have been as abrasive agents for cleaning teeth, such as pumice, powdered marble, bone and shell.<sup>69</sup> Today a wide range of insoluble inorganic materials such as silica, metal oxides, carbonates, clays, and phosphates are used, with silica and calcium carbonate being the preferred material in most commercial products.<sup>70</sup>

The main factor that limits the choice of materials (after its toxicity and biocompatibility to humans) is its hardness, a measure of how a material will resist a deformation (such as a scratch or indent) when a force is applied. When two objects come into contact, the difference in hardness of the materials of the objects will affect what happens, such as one object scratching (removing material from- or deforming) the other, or both scratching each other, and to what degree.<sup>71</sup> For dental applications one therefore wants an abrasive which is hard enough to be able to remove tartar and precipitated minerals, whilst minimising the damage it causes to the tooth surface which it is cleaning. As the hardness of enamel and dentin differ, there is a trade-off when designing a toothpaste between the relative damage caused to the enamel and dentin, and the product's cleaning ability.

As there is a limit in the choice of materials which can feasibly be used in commercial applications, it is desirable to look at other factors which affect abrasive properties. In a slurry system, such as the one created by toothpaste being used in the mouth, abrasives move through a viscous liquid before making contact with the tooth surface. Larger particles having higher velocities and therefore generally remove (abrade) more material, making them more effective for the purpose.<sup>72</sup> This is of course subject to an upper boundary as larger particles will connect with a proportionally smaller surface area, and eventually this factor will outweigh the usefulness an increase in velocity provides at a given concentration of abrasive material in a product. Additionally, the method of how abrasives are applied to the surface also poses a limit on particle size. As a toothbrush is generally used to move the abrasive particles in toothpaste



over the tooth surface, particles in these formulations must be able to be trapped between the bristles of the toothbrush, making particles with all dimensions larger than 10  $\mu\text{m}$  undesirable for this purpose.

Particle morphology is another factor which determines how abrasive a material is. It is generally believed that particles with irregular forms are more abrasive than those with homogenous arrangements of their individual agglomerated parts or grains.<sup>73</sup> Particles with rough surfaces will have a relatively small area of contact with the surface, resulting in a higher pressure at the area of contact and therefore cause a higher level of abrasion. It is difficult to directly compare to what extent the differences in morphology are affecting the abrasive properties of particles as opposed to the material of the particle, as certain particle morphologies can only (with currently available fabrication methods) be obtained with certain materials.

If you move a particle over a surface by exerting horizontal force you can imagine its movement proceeding by one of two main mechanisms. The particle could slide on the surface, where contact is maintained between the surface and the points balancing the particle. The particle could also roll, where new parts of the particle are brought into contact with the surface. In both of these cases rough particles will cause micro-regions of high pressure. If particles with flat or rounded surfaces are used the contact area is increased and the pressure exerted on the surface decreased. Although this roughness will play a part in the effectiveness of the abrasive, for dental cleaning a flatter particle might still be effective. The accumulated debris on the tooth will be relatively non-flat compared to the tooth surface, so a flat particle which is sliding on a flat surface would still be able to exert a large force when colliding with the debris.

The original inspiration for this project was to look at the cleaning ability of rod-like particles, as it was believed that they might exhibit less damage to the tooth surface by rolling smoothly or sliding over the surface.

### 4.1.3 Evaluation of dentifrice performance

The performance of dentifrices are evaluated in industry by three values; the Pellicle cleaning ratio (PCR), relative dentin abrasion (RDA), and the cleaning efficiency index (CEI).<sup>74</sup> The Pellicle Cleaning Ratio (PCR) is a value of how much a product cleans teeth, using the Stookey method.<sup>75</sup> The Stookey method measures the brightness of a stained surface before and after it has been cleaned by the product being evaluated, as well as after the surface has had all stain mechanically removed. Typically, human or bovine teeth which have been stained by tea and coffee are used as the surface to be cleaned.

Relative Dentin Abrasion (RDA) is a value of how abrasive a product is to teeth, measured by the amount of radioactive wash-off produced from irradiated root dentin which is brushed with the tested product.<sup>76</sup> The Cleaning Efficiency Index (CEI) combines PCR and RDA to emphasize the importance of stain removal as well as low tooth abrasion, and is calculated according to the equation<sup>77</sup>:

$$CEI = \frac{(RDA + PCR - 50)}{RDA}$$

Ideally a product will have a high PCR, a low RDA, and therefore a high CEI value, which indicates a product that removes dirt from the surface of teeth whilst not damaging the surface itself.

## 4.2 Experimental Section

Cows teeth mounted to epoxy blocks were used to test cleaning of several synthesised particles. These blocks were stained in a mixture containing instant coffee, instant tea, mucin, soy broth, and ferric chloride by staff at Unilever Port Sunlight.

Particles were prepared for testing by mixing them into a slurry containing water, particles, and abrasive-free toothpaste base. A control was prepared by making a slurry of commercially available toothpaste (SIGNAL White System, containing silica abrasive particles) with water. The slurry of tested particles contained 5 wt% abrasive material, whilst the control slurry contained 20 wt% abrasive material.

Cleaning tests were performed using toothbrush heads mounted onto a SDLAtlas Martindale M235 textile abrasion tester. Color measurements were done with Minolta colorimeter (recording the 'L\*a\*b' color space).

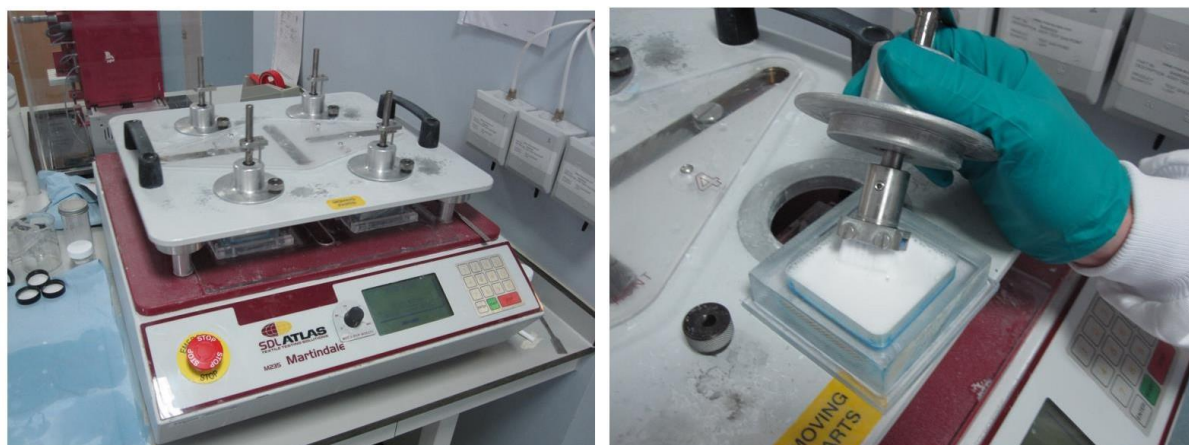


***Figure 26 – (Left) Abrasion tester apparatus. (Right) Tooth block covered in slurry and mounted toothbrush being held.***

First color measurements were done on the teeth after they had been stained and gently washed with water. The teeth were then mounted into containers and had 20 ml particle/toothpaste slurry poured over them before being brushed with 800 strokes over 5 minutes. The teeth were then rinsed with water and dried before having their color measured again. Finally, the teeth were polished with flour of pumice on a Buehler Metaserv 2000 to remove any remaining stain before having a final color measurement taken. Eight teeth were used to test each abrasive.

The Lab color space represents in a color with three values:  $L^*$ ,  $a^*$ , and  $b^*$ . The  $L^*$  component is a measure of lightness, which in this experiment is used as a value for the ‘whiteness’ of the tooth. This test provide three lightness values; when the tooth is dirty before it has been cleaned ( $L^*_{(1)}$ ), after the tooth has been brushed ( $L^*_{(2)}$ ), and when all the stain has been removed by polishing ( $L^*_{(3)}$ ). The amount of dirt removed (measured by the increase in brightness of the tooth) compared to total amount of removable dirt can be calculated by:

$$PCR = \frac{L^*_{(3)} - L^*_{(2)}}{L^*_{(3)} - L^*_{(1)}}$$

Where a value of 0 indicates that brushing did not increase the brightness of the tooth at all, and a 1 indicates that polishing the tooth did not make it any brighter than brushing alone.

### 4.3 Results and Discussion

Synthesised and commercially acquired calcium carbonate and silica particles had their cleaning ability measure using the Stookey method and were compared to a commercially available toothpaste standard. Figures 27-30 show the compiled results obtained from 8 cleaning tests of each sample. Table 1 shows the identity of each sample being tested. Figure 31 shows micrographs of some of the samples being tested. It is to be noted that some samples tested were different batches of material synthesised in the same manner (which is explicitly stated in the table), and as such only one micrograph is shown for each of these groupings.

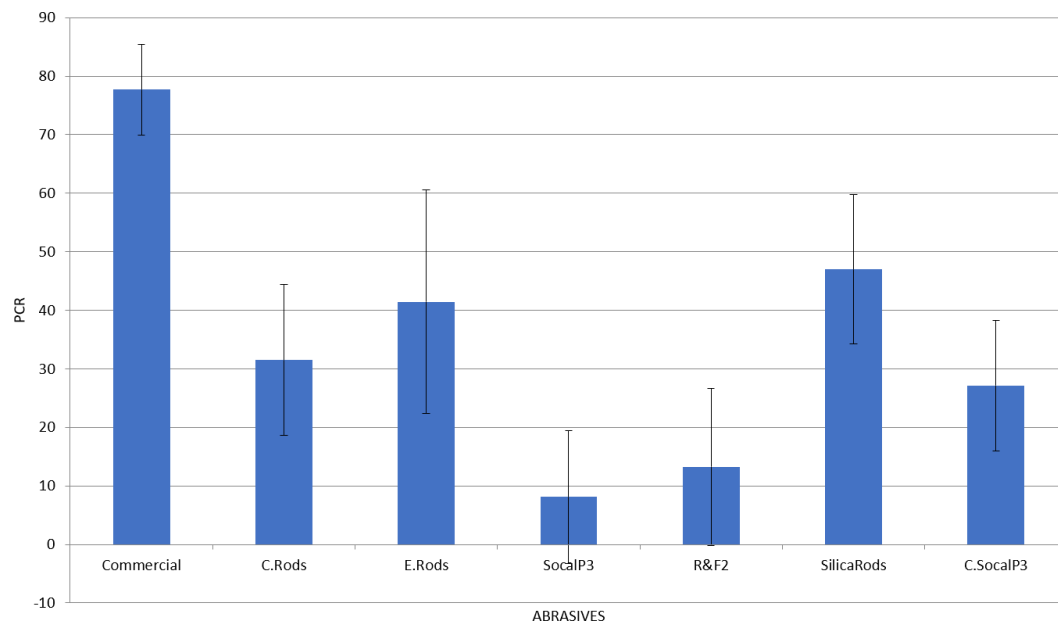


**Figure 27 – Cleaning results ‘A’ of abrasives**

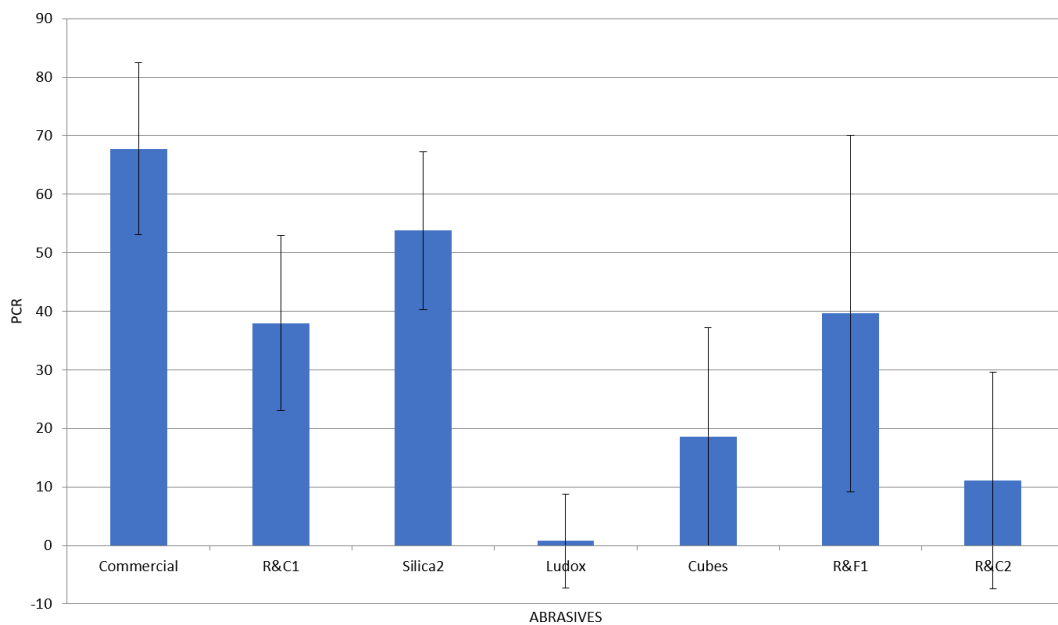


**Figure 28 – Cleaning results ‘B’ of abrasives**



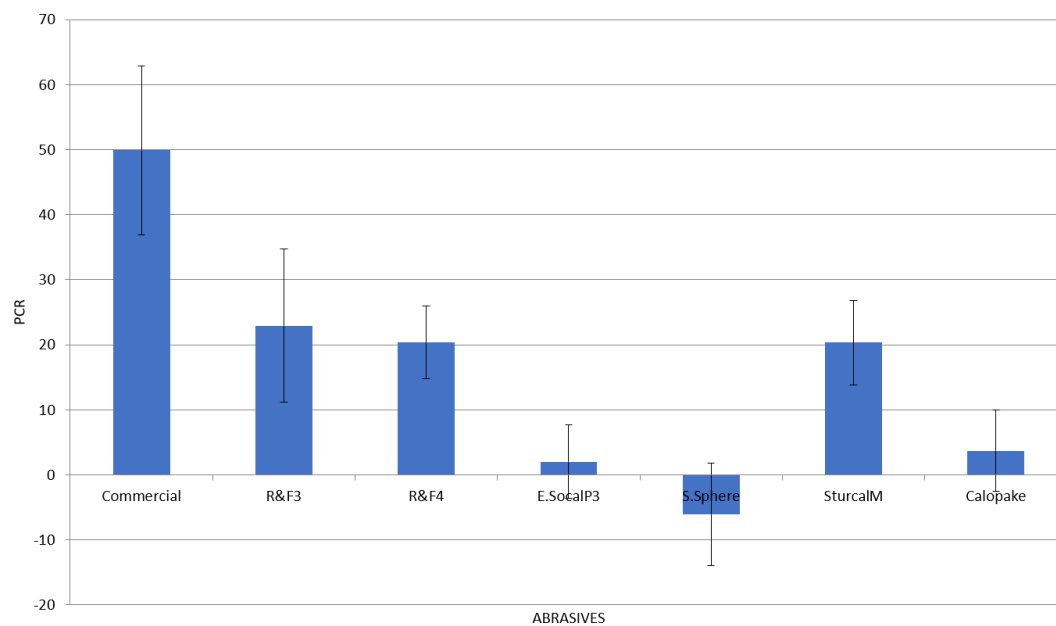


**Figure 29 – Cleaning results ‘C’ of abrasives**

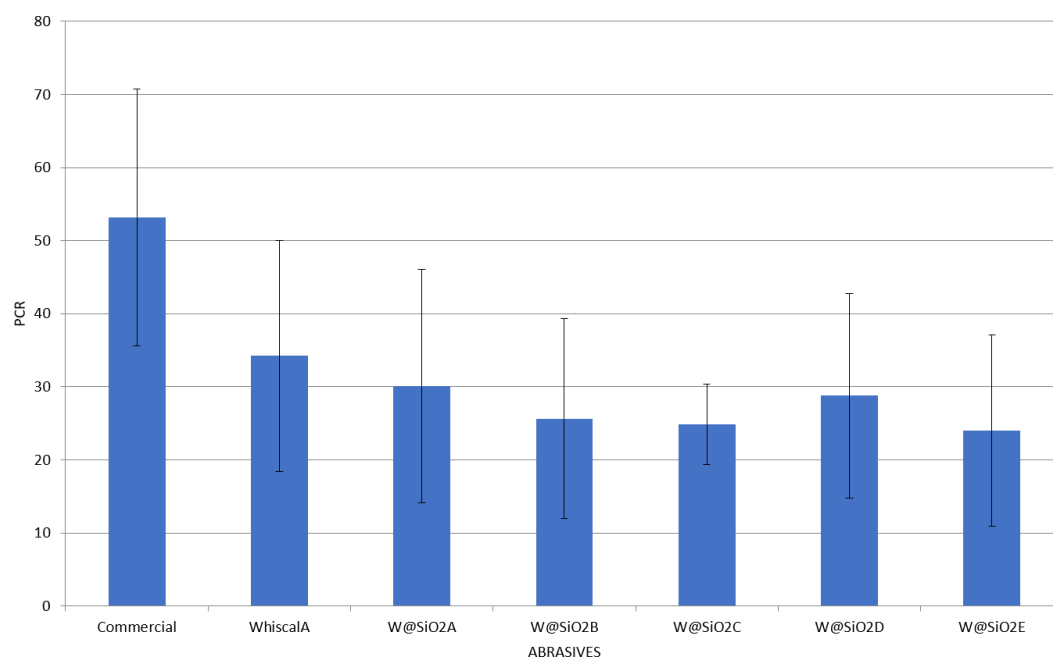


**Figure 30 – Cleaning results ‘D’ of abrasives**

<b>Abrasive Identity</b>	<b>Description</b>	<b>Image in figure X</b>
<b>Commercial</b>	Commercial silica toothpaste	Not shown
<b>Cubes</b>	CaCO <sub>3</sub> cubes	A
<b>R&amp;C 1,2</b>	CaCO <sub>3</sub> rods and cubes	C
<b>R&amp;F 1,2,3,4</b>	CaCO <sub>3</sub> rods and flowers	B
<b>C.Rods</b>	SiO <sub>2</sub> coated CaCO <sub>3</sub> rods	D
<b>E.Rods</b>	Hollow SiO <sub>2</sub> rods	Not shown, similar to D
<b>SocalP3</b>	Commercial PCC	J
<b>C.SocaP3</b>	SiO <sub>2</sub> coated SocalP3	Not shown, similar to J
<b>E.SocalP3</b>	Hollow SiO <sub>2</sub> shell from SocalP3	K
<b>S.Sphere</b>	Silica spheres	I
<b>Silica2</b>	Rounded silica particles	G
<b>SilicaRods</b>	Silica rods	H
<b>Ludox</b>	Commercial 12nm silica spheres	Not shown
<b>SturcalM</b>	Commercial PCC	F
<b>Calopake</b>	Commercial PCC	E
<b>WhiscalA</b>	Commercial PCC rods	L
<b>WhiscalA@SiO<sub>2</sub></b> A,B,C,D,E	SiO <sub>2</sub> coated Whiscal A	Not shown, similar to L

*Table 1 – Identity of materials in cleaning tests*

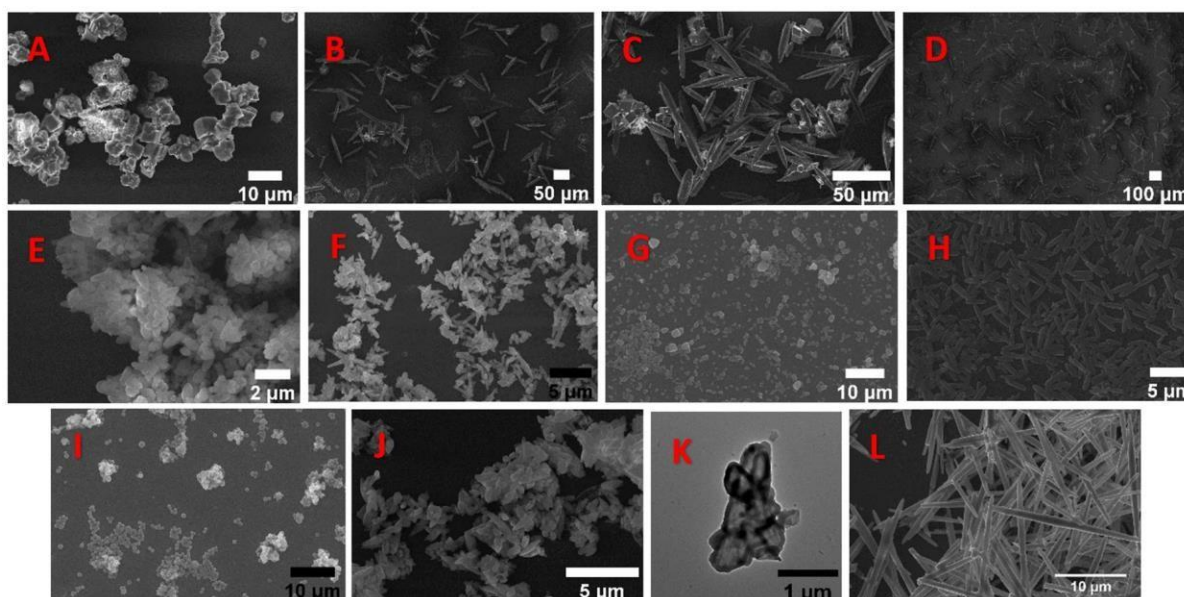



**Figure 31 – Micrographs of materials in cleaning tests. (A) Cubes. (B) Rods and flowers. (C) Rods and cubes. (D) Coated rods. (E) Calopake. (F) Sturcal M. (G) Silica 2. (H) Silica rods. (I) Silica spheres. (J) Socal P3. (K) Etched Socal P3. (L) Whiscal A.**

*Declaration: Synthesis and imaging of Socal P3 particles (SocalP3, C.SocalP3, E.SocalP3) was done by Robert Young. Synthesis and imaging of pure silica particles (S.Sphere, Silica2, Silica Rods) was done by Christopher Parkins*

A notable feature of the obtained graphs is the large error bars (showing the range of obtained PCR values for each abrasive), as well as some experiments giving negative PCR values (indicating tooth surfaces were less bright as a result of the cleaning experiment). The bovine teeth being used as the cleaning surface had been used several times before for the same purpose, and as such have been stained and cleaned several times. This resulted in the deterioration of the surface as well as permanent staining, both of which will increase the error of obtained results. As a result of this error only qualitative conclusions can be drawn from the results.


In each of the four trials the commercial toothpaste always cleaned best. One major reason for this occurring is that the total amount of abrasive material was roughly four times as high in the commercial sample compared to slurries made from added abrasives (20 wt% vs. 5 wt% in accordance with the followed protocol).



Socal P3, Ludox, silica spheres, calopake, and etched Socal P3 all received PCR scores of under 10%. Both the ludox and silica spheres were expected to receive low scores due to their spherical morphology exhibiting very low roughness. Coated Socal P3 cleaned moderately well (25% PCR) whilst uncoated or etched it received a much lower score. The increase in PCR between the uncoated and coated sample can be rationalised as being due to the change in particle surface chemistry from CC to silica. As this remains true for the etched particle there must be another factor resulting in the decrease in PCR. It is possible that the mechanical force exerted on the hollow particle during brushing breaks them, forming smaller shards of silica which clean the surface less well than when the larger particles are intact. This trend was not seen for the coated and etched  $\text{CaCO}_3$  rods, where the etched particle cleaned roughly the same (40% PCR) amount as the coated one (30% PCR). This could be due to the hollow particles not breaking, or the fragments formed remaining quite large and still suitable for cleaning.

Sturcal M, which received a modest PCR of 20%, and Calopake (4% PCR), are both formed of agglomerations of smaller CC particles, which are comparable in size between the samples. The morphology of Sturcal M however appears rougher, with sharper angles, whilst Calopake shows more smooth features, which could account for the large difference in PCR scores. The various synthesised  $\text{CaCO}_3$  particles received scores of between 10-40% PCR, with no consistent trends being shown between the various morphologies. It seems that the larger  $\text{CaCO}_3$  particles which were synthesised, as opposed to the smaller Sturcal M and Calopake agglomerates, cleaned better, which is most likely due to the larger size. No conclusions can be drawn however of the impact morphology had in the differences of cleaning ability.

The results shown in Figure X, where only one morphology (rods) was used, further skews what conclusions can be drawn. Whiscal A is a rod-like  $\text{CaCO}_3$  particle, whilst all other samples were silica coated version of Whiscal A with varying thicknesses of the silica shell, as



well as some containing pendant alkyl chains on the silica shell. Whiscal A received the highest PCR (35%) whilst all the coated samples were lower. This is in contrast with what would be expected due to the difference in material hardness. However, as all the error bars from the summarised results overlap from these measurements it is difficult to draw any meaningful conclusion.

#### **4.4 Conclusions**

Although no strong conclusions could be drawn from the obtained results about the effect of particle morphology on cleaning ability, the ability of larger particles to clean better than smaller ones is apparent. Spherical particles are also shown to clean worse than other particle morphologies. Without having performed RDA measurements it is difficult to conclude whether the differences in cleaning are due to the particles removing the plaque layer from the tooth surface, or due to generally damaging the tooth surface itself and exposing underlying material. The design of the Stookey test itself seems flawed as the nature of using irregular surfaces which differ from sample to sample does not allow for consistent measures with otherwise consistent conditions.

---

## **CHAPTER 5**

### **“Conclusions and Future Recommendations”**

In this chapter conclusions of all presented work are summarised, and recommendations for further work into the discussed areas are presented.

## General conclusions


A novel system for the synthesis of dagger-like vaterite calcium carbonate particles was shown. Linear polyols exerted a strong effect on the obtained morphologies as well as polymorphic selection.

Calcium carbonate particles were successfully modified via surface addition of silica and polymers, as well as being used as sacrificial templates to make sodium fluoride particles.

Various calcium carbonate and silica particles were tested for their ability to clean teeth using the Stookey method. Whilst some conclusions about the effect that particle properties such as morphology, size, and material had on cleaning ability, large errors in the obtained data prevented useful explanations from being obtained.

## Recommendations

Whilst it is unknown exactly why the use of polyols (and the trends between the different polyols) showed the observed effects, it is believed that this could be due to a change in saturation of the various reaction components, and as a result the changing supersaturation affects the nucleation and growth of the calcium carbonate particles. This could be reliant on both the viscosity of the different polyol solutions, as well as the chemical nature of the polyols themselves. To examine this online viscosity measurements of the reactions would help to see if viscosity plays an important role in the reactions. It would also be interesting for this data to be used to look at the induction time of the crystallization (from when ACC is formed and viscosity increases, to its disappearance and solution viscosity decrease).



Further data on the effect polyols have on growing calcium carbonate crystals is needed. Online XRD and Raman measurements of the reactions would allow crystallite size and polymorph to be followed. Due to the timescales involved, with the appearance and disappearance of ACC occurring over the scale of minutes and seconds, this would require the use of a neutron source for XRD measurements.

XPS and molecular dynamic simulations of the various polyols on ACC, vaterite, aragonite, and calcite surfaces would help to see how alcohol binding to the growing crystals affects their growth. This could help elucidate whether there is any significant binding between the alcohol groups and the growing crystal face, and how this is affecting crystal growth.

Combinations of various polyols (for example ethylene glycol + sorbitol, glycerol + xylitol etc.) could be used to see if it is the chemical structure of the polyols themselves which drive the shown changes, or whether other factors (such as viscosity, by matching viscosities of reactions using various combinations of polyols) are dominant.

The use of liquid TEM could be used to visually examine the nucleation and growth of calcium carbonate crystals, which would be particularly powerful in examining how the polyols affect the morphology of the crystals.

One line of inquiry which was not looked at in this work is the chiral nature of the polyols used. If there is significant bonding between the alcohol groups of the polyols and the surface of the calcium carbonate particles, it would be possible for different stereoisomers of polymers to produce particles of various morphologies due to changes in how they bond with the crystal.



## MATERIALS AND ANALYTIC METHODS

### Materials

All chemicals were used as received unless otherwise specified.

All monomers (AA, MAA, DVB) were passed through a column of basic alumina immediately before use to remove inhibitors.

AIBN was recrystallized in methanol before use.

Erythritol, xylitol, and sorbitol were dried under vacuum before use.

Calcium chloride (fused, granular), sodium carbonate (anhydrous), 35% ammonia solution, 37% hydrochloric acid, and glycerol (99.5%) were received from Fischer Scientific.

Methacrylic acid (99%), tetraethyl orthosilicate (98%), divinylbenzene (80%), sodium fluoride ( $\geq 99\%$ ), acetone ( $\geq 99\%$ ), methanol ( $\geq 99.6\%$ ), D-sorbitol ( $\geq 98\%$ ), ethylene glycol ( $> 99\%$ ), and acetic acid (glacial,  $\geq 99.85\%$ ) were received from Sigma-Aldrich.

Azobisisobutyronitrile, ethanol (absolute, 99.85%), and acetonitrile (99.9%) were received from VWR International.

‘Whiscal A’ precipitated calcium carbonate was donated by Maruo Calcium Co.

‘Socal P3’ precipitated calcium carbonate was received from Solvay.

‘Calopake’ and ‘Sturcal M’ precipitated calcium carbonate was received from Specialty Minerals.

Xylitol was received from Total Sweet.

Erythritol was received from Pure Sweet.

Deionized water was obtained using a Milli-Q filtration system from Merck Millipore.

### Analytic methods

#### Scanning electron microscopy (SEM)

The sample to be imaged is added onto a silica wafer which is adhered to an aluminium stub. The sample is coated in a carbon film before being imaged with a Zeiss SUPRA 55-VP or Zeiss Gemini scanning electron microscope.

#### Transmission electron microscopy (TEM)

The sample is added to a copper grid before being imaged with a JEOL 2000fx or JEOL 2100 transmission electron microscope.

### **Uniaxial compression testing**

2.5 cm<sup>3</sup> of dry powder is added to a KBr press sample holder with a 35 g aluminium rod placed on top of the sample. A Shimadzu AGS-X tensile tester is then used to press the aluminium rod down onto the powder at a fixed compression rate of 10 mm min<sup>-1</sup> until the compressive force reaches 500 N or 1000 N.

### **Fluoride ion selective electrode (FISE) measurements**

A Nico2000 ELIT 8821 Fluoride Ion-Selective Electrode probe, connected to an Orion Star a215 pH/conductivity Benchtop Meter, is inserted into the fluoride ion containing reaction mixture. Measurements are taken every 5s.

### **X-ray crystal diffraction measurements (XRD)**

Powder XRD measurements were performed with a Panalytical X-Pert Pro MPD using a copper diffraction source and spinning stage.

Literature references of pure crystal samples from the International Centre for Diffraction Data (ICDD) were used to identify peaks in spectra of examined materials. 162480-ICSD-PXRD was used for vaterite. 166364-ICSD-PXRD was used for calcite. 170225-ICSD-PXRD was used for aragonite. 52754-ICSD was used for sodium fluoride.

### **Energy-dispersive X-ray spectroscopy (EDX)**

EDX measurements were performed using an Oxford Instruments energy-dispersive X-ray spectrometer attached to a Zeiss SUPRA 55-VP scanning electron microscope.

## REFERENCES

- (1) Vetter, a. F.; Swanson, P. a. Particle Morphology Applied To Characterizing Abrasive Materials. *Part. Sci. Technol.* **1983**, *1* (2), 127–138. <https://doi.org/10.1080/02726358308906360>.
- (2) O’Sullivan, M.; Zhang, Z.; Vincent, B. Silica-Shell/Oil-Core Microcapsules with Controlled Shell Thickness and Their Breakage Stress. *Langmuir* **2009**, *25* (14), 7962–7966. <https://doi.org/10.1021/la9006229>.
- (3) Khomane, R. B.; Kulkarni, B. D. I NTERNATIONAL J OURNAL OF C HEMICAL Nanoreactors ForNanostructured Materials Nanoreactors for Nanostructured Materials. *Int. J. Chem. React. Eng.* **2008**, *6*.
- (4) Tronc, F.; Li, M.; Lu, J.; Winnik, M. a.; Kaul, B. L.; Graciet, J. C. Fluorescent Polymer Particles by Emulsion and Miniemulsion Polymerization. *J. Polym. Sci. Part A Polym. Chem.* **2003**, *41* (6), 766–778. <https://doi.org/10.1002/pola.10619>.
- (5) Thompson, R. C.; Moore, C. J.; Saal, F. S.; Swan, S. H. Plastics , the Environment and Human Health : Current Consensus and Future Trends. *Phil. Trans. R. Soc. B* **2009**, *364*, 2153–2166. <https://doi.org/10.1098/rstb.2009.0053>.
- (6) Wolf, S. E.; Gower, L. B. *New Perspectives on Mineral Nucleation and Growth*; 2017. [https://doi.org/10.1007/978-3-319-45669-0\\_3](https://doi.org/10.1007/978-3-319-45669-0_3).
- (7) Karthika, S.; Radhakrishnan, T. K.; Kalaichelvi, P. A Review of Classical and Nonclassical Nucleation Theories. *Cryst. Growth Des.* **2016**, *16* (11), 6663–6681. <https://doi.org/10.1021/acs.cgd.6b00794>.
- (8) Lutsko, J. F. How Crystals Form: A Theory of Nucleation Pathways. *arXiv* **2019**, 1–9.
- (9) Kim, Y. Y.; Schenk, A. S.; Ihli, J.; Kulak, A. N.; Hetherington, N. B. J.; Tang, C. C.; Schmah, W. W.; Griesshaber, E.; Hyett, G.; Meldrum, F. C. A Critical Analysis of Calcium Carbonate Mesocrystals. *Nat. Commun.* **2014**, *5*. <https://doi.org/10.1038/ncomms5341>.
- (10) Dickinson, S. R.; Henderson, G. E.; McGrath, K. M. Controlling the Kinetic versus Thermodynamic Crystallisation of Calcium Carbonate. *J. Cryst. Growth* **2002**, *244* (3–4), 369–378. [https://doi.org/10.1016/S0022-0248\(02\)01700-1](https://doi.org/10.1016/S0022-0248(02)01700-1).
- (11) Wirnereux, S. M. De; Lille, U. De; Cnrs, E. P.; Wirnereux, F.-. Calcium Carbonate Production of a Dense Population of the Brittle Star Ophiothrix Fragilis ( Echinodermata : Ophiuroidea ): C-2. **1998**, No. Anonymous 1988.
- (12) Sawada, K. The Mechanisms of Crystallization and Transformation of Calcium Carbonates. *Pure Appl. Chem.* **1997**, *69* (5), 921–928. <https://doi.org/10.1351/pac199769050921>.
- (13) Runnegar, B. Shell Microstructures of Cambrian Molluscs Replicated by Phosphate. *Alcheringa An Australas. J. Palaeontol.* **1985**, *9* (4), 245–257. <https://doi.org/10.1080/03115518508618971>.
- (14) Vecht, A.; Ireland, T. G. The Role of Vaterite and Aragonite in the Formation of Pseudo-Biogenic Carbonate Structures: Implications for Martian Exobiology. *Geochim. Cosmochim. Acta* **2000**, *64* (15), 2719–2725. [https://doi.org/10.1016/S0016-7037\(00\)00381-1](https://doi.org/10.1016/S0016-7037(00)00381-1).

- (15) Meiron, O. E.; Bar-David, E.; Aflalo, E. D.; Shechter, A.; Stepensky, D.; Berman, A.; Sagi, A. Solubility and Bioavailability of Stabilized Amorphous Calcium Carbonate. *J. Bone Miner. Res.* **2011**, *26* (2), 364–372. <https://doi.org/10.1002/jbmr.196>.
- (16) Addadi, L.; Raz, S.; Weiner, S. Taking Advantage of Disorder: Amorphous Calcium Carbonate and Its Roles in Biomineralization. *Adv. Mater.* **2003**, *15* (12), 959–970. <https://doi.org/10.1002/adma.200300381>.
- (17) Threlfall, T. Structural and Thermodynamic Explanations of Ostwald's Rule. *Org. Process Res. Dev.* **2003**, *7* (6), 1017–1027. <https://doi.org/10.1021/op030026l>.
- (18) Steefel, C. I.; Van Cappellen, P. A New Kinetic Approach to Modeling Water-Rock Interaction: The Role of Nucleation, Precursors, and Ostwald Ripening. *Geochim. Cosmochim. Acta* **1990**, *54* (10), 2657–2677. [https://doi.org/10.1016/0016-7037\(90\)90003-4](https://doi.org/10.1016/0016-7037(90)90003-4).
- (19) Sarkar, A.; Mahapatra, S. Mechanism of Unusual Polymorph Transformations in Calcium Carbonate: Dissolution-Recrystallization vs Additive-Mediated Nucleation. *J. Chem. Sci.* **2012**, *124* (6), 1399–1404. <https://doi.org/10.1007/s12039-012-0339-9>.
- (20) Agarwal, P.; Berglund, K. A. In Situ Monitoring of Calcium Carbonate Polymorphs during Batch Crystallization in the Presence of 2003. **2003**, 0–5.
- (21) Bots, P.; Benning, L. G.; Rodriguez-Blanco, J.-D.; Roncal-Herrero, T.; Shaw, S. Mechanistic Insights into the Crystallization of Amorphous Calcium Carbonate (ACC). *Cryst. Growth Des.* **2012**, *12* (7), 3806–3814. <https://doi.org/10.1021/cg300676b>.
- (22) Rieger, J.; Frechen, T.; Cox, G.; Heckmann, W.; Schmidt, C.; Thieme, J. Precursor Structures in the Crystallization/Precipitation Processes of CaCO<sub>3</sub> and Control of Particle Formation by Polyelectrolytes. *Faraday Discuss.* **2007**, *136*, 265–277. <https://doi.org/10.1039/b701450c>.
- (23) Ogino, T.; Suzuki, T.; Sawada, K. THE RATE AND MECHANISM OF POLYMORPHIC TRANSFORMATION OF CALCIUM CARBONATE IN WATER Takeshi OGINO, Toshio SUZUKI and Kiyoshi SAWADA. *J. Cryst. Growth* **1990**, *100*, 159–167.
- (24) Noel, E. H.; Kim, Y.-Y.; Charnock, J. M.; Meldrum, F. C. Solid State Crystallization of Amorphous Calcium Carbonate Nanoparticles Leads to Polymorph Selectivity. *CrystEngComm* **2013**, *15* (4), 697. <https://doi.org/10.1039/c2ce26529j>.
- (25) Ihli, J.; Wong, W. C.; Noel, E. H.; Kim, Y. Y.; Kulak, A. N.; Christenson, H. K.; Duer, M. J.; Meldrum, F. C. Dehydration and Crystallization of Amorphous Calcium Carbonate in Solution and in Air. *Nat. Commun.* **2014**, *5*, 1–10. <https://doi.org/10.1038/ncomms4169>.
- (26) Gal, A.; Habraken, W.; Gur, D.; Fratzl, P.; Weiner, S.; Addadi, L. Calcite Crystal Growth by a Solid-State Transformation of Stabilized Amorphous Calcium Carbonate Nanospheres in a Hydrogel. *Angew. Chemie - Int. Ed.* **2013**, *52* (18), 4867–4870. <https://doi.org/10.1002/anie.201210329>.
- (27) Radha, A. V.; Forbes, T. Z.; Killian, C. E.; Gilbert, P. U. P. A.; Navrotsky, A. Transformation and Crystallization Energetics of Synthetic and Biogenic Amorphous Calcium Carbonate. *Proc. Natl. Acad. Sci.* **2010**, *107* (38), 16438–16443. <https://doi.org/10.1073/pnas.1009959107>.
- (28) Zhang, Z.; Xie, Y.; Xu, X.; Pan, H.; Tang, R. Transformation of Amorphous Calcium Carbonate into Aragonite. *J. Cryst. Growth* **2012**, *343* (1), 62–67. <https://doi.org/10.1016/j.jcrysgro.2012.01.025>.
- (29) Gorna, K.; Muñoz-Espí, R.; Gröhn, F.; Wegner, G. Bioinspired Mineralization of

- Inorganics from Aqueous Media Controlled by Synthetic Polymers. *Macromol. Biosci.* **2007**, *7*, 163–173. <https://doi.org/10.1002/mabi.200600209>.
- (30) Beniash, E.; Aizenberg, J.; Addadi, L.; Weiner, S. Amorphous Calcium Carbonate Transforms into Calcite during Sea Urchin Larval Spicule Growth. *Proc. R. Soc. B Biol. Sci.* **1997**, *264* (1380), 461–465. <https://doi.org/10.1098/rspb.1997.0066>.
  - (31) Abebe, M.; Hedin, N.; Bacsik, Z. Spherical and Porous Particles of Calcium Carbonate Synthesized with Food Friendly Polymer Additives. *Cryst. Growth Des.* **2015**, *15* (8), 3609–3616. <https://doi.org/10.1021/cg501861t>.
  - (32) Ahmed, J.; Menaka; Ganguli, A. K. Controlled Growth of Nanocrystalline Rods, Hexagonal Plates and Spherical Particles of the Vaterite Form of Calcium Carbonate. *CrystEngComm* **2009**, *11* (5), 927–932. <https://doi.org/10.1039/b820928f>.
  - (33) Chen, X.; Tang, Q.; Liu, D.; Hu, W.; Dan, Y. Preparation and Characterization of Three-Dimensional Chrysanthemum Flower-like Calcium Carbonate. *J. Wuhan Univ. Technol. Sci. Ed.* **2012**, *27* (4), 708–714. <https://doi.org/10.1007/s11595-012-0533-0>.
  - (34) Yao, H. Bin; Ge, J.; Mao, L. B.; Yan, Y. X.; Yu, S. H. 25th Anniversary Article: Artificial Carbonate Nanocrystals and Layered Structural Nanocomposites Inspired by Nacre: Synthesis, Fabrication and Applications. *Adv. Mater.* **2014**, *26* (1), 163–188. <https://doi.org/10.1002/adma.201303470>.
  - (35) Nudelman, F.; Sommerdijk, N. a J. M. Biomineralization as an Inspiration for Materials Chemistry. *Angew. Chem. Int. Ed. Engl.* **2012**, *51* (27), 6582–6596. <https://doi.org/10.1002/anie.201106715>.
  - (36) Addadi, L.; Joester, D.; Nudelman, F.; Weiner, S. Mollusk Shell Formation: A Source of New Concepts for Understanding Biomineralization Processes. *Chem. - A Eur. J.* **2006**, *12* (4), 980–987. <https://doi.org/10.1002/chem.200500980>.
  - (37) Kitamura, M. Strategy for Control of Crystallization of Polymorphs. *CrystEngComm* **2009**, *11* (6), 949. <https://doi.org/10.1039/b809332f>.
  - (38) Kim, Y.-Y.; Ganesan, K.; Yang, P.; Kulak, A. N.; Borukhin, S.; Pechook, S.; Ribeiro, L.; Kröger, R.; Eichhorn, S. J.; Armes, S. P.; Pokroy, B.; Meldrum, F. C. An Artificial Biomineral Formed by Incorporation of Copolymer Micelles in Calcite Crystals. *Nat. Mater.* **2011**, *10* (11), 890–896. <https://doi.org/10.1038/nmat3103>.
  - (39) Meldrum, F. C.; Cölfen, H. Controlling Mineral Morphologies and Structures in Biological and Synthetic Systems. *Chem. Rev.* **2008**, *108* (11), 4332–4432. <https://doi.org/10.1021/cr8002856>.
  - (40) Beck, R.; Andreassen, J. P. The Onset of Spherulitic Growth in Crystallization of Calcium Carbonate. *J. Cryst. Growth* **2010**, *312* (15), 2226–2238. <https://doi.org/10.1016/j.jcrysgro.2010.04.037>.
  - (41) Chen, S.; Yu, S.; Jiang, J.; Li, F.; Liu, Y. Polymorph Discrimination of CaCO<sub>3</sub> Mineral in an Ethanol / Water Solution : Formation of Complex Vaterite Superstructures and Aragonite Rods. **2006**, No. 7, 115–122.
  - (42) Andreassen, J. P. Formation Mechanism and Morphology in Precipitation of Vaterite - Nano-Aggregation or Crystal Growth? *J. Cryst. Growth* **2005**, *274* (1–2), 256–264. <https://doi.org/10.1016/j.jcrysgro.2004.09.090>.
  - (43) Sand, K. K.; Rodriguez-Blanco, J. D.; Makovicky, E.; Benning, L. G.; Stipp, S. L. S. Crystallization of CaCO<sub>3</sub> in Water-Alcohol Mixtures: Spherulitic Growth, Polymorph Stabilization, and Morphology Change. *Cryst. Growth Des.* **2012**, *12* (2), 842–853. <https://doi.org/10.1021/cg2012342>.
  - (44) Manoli, F.; Dalas, E. Spontaneous Precipitation of Calcium Carbonate in the Presence

- of Ethanol, Isopropanol and Diethylene Glycol. *J. Cryst. Growth* **2000**, 218 (2), 359–364. [https://doi.org/10.1016/S0022-0248\(00\)00560-1](https://doi.org/10.1016/S0022-0248(00)00560-1).
- (45) Li, Q.; Ding, Y.; Li, F.; Xie, B.; Qian, Y. Solvothermal Growth of Vaterite in the Presence of Ethylene Glycol, 1,2-Propanediol and Glycerin. *J. Cryst. Growth* **2002**, 236 (1–3), 357–362. [https://doi.org/10.1016/S0022-0248\(01\)02130-3](https://doi.org/10.1016/S0022-0248(01)02130-3).
  - (46) Kim, I. W.; Robertson, R. E.; Zand, R. Effects of Some Nonionic Polymeric Additives on the Crystallization of Calcium Carbonate. *Cryst. Growth Des.* **2005**, 5 (2), 513–522. <https://doi.org/10.1021/cg049721q>.
  - (47) Hosoda, N.; Sugawara, A.; Kato, T. Template Effect of Crystalline Poly(Vinyl Alcohol) for Selective Formation of Aragonite and Vaterite CaCO<sub>3</sub> Thin Films. *Macromolecules* **2003**, 36 (17), 6449–6452. <https://doi.org/10.1021/ma025869b>.
  - (48) Bovet, N.; Yang, M.; Javadi, M. S.; Stipp, S. L. S. Interaction of Alcohols with the Calcite Surface. *Phys. Chem. Chem. Phys.* **2015**, 17 (5), 3490–3496. <https://doi.org/10.1039/c4cp05235h>.
  - (49) Trushina, D. B.; Bukreeva, T. V.; Antipina, M. N. Size-Controlled Synthesis of Vaterite Calcium Carbonate by the Mixing Method: Aiming for Nanosized Particles. *Cryst. Growth Des.* **2016**, 16 (3), 1311–1319. <https://doi.org/10.1021/acs.cgd.5b01422>.
  - (50) Qi, R. J.; Zhu, Y. J. Microwave-Assisted Synthesis of Calcium Carbonate (Vaterite) of Various Morphologies in Water - Ethylene Glycol Mixed Solvents. *J. Phys. Chem. B* **2006**, 110 (16), 8302–8306. <https://doi.org/10.1021/jp060939s>.
  - (51) Ballard, N.; Bon, S. A. F. Hybrid Biological Spores Wrapped in a Mesh Composed of Interpenetrating Polymer Nanoparticles as “Patchy” Pickering Stabilizers. *Polym. Chem.* **2011**, 2 (4), 823–827. <https://doi.org/10.1039/C0PY00335B>.
  - (52) Stober, W. E. R. N. E. R. Controlled Growth of Monodisperse Silica Spheres in the Micron Size Range 1. **1968**, 69, 62–69.
  - (53) Kondo, A.; Kamura, H.; Higashitani, K. Development and Application of Thermo-Sensitive Magnetic Immunomicrospheres for Antibody Purification. *Appl. Microbiol. Biotechnol.* **1994**, 41 (1), 99–105. <https://doi.org/10.1007/BF00166089>.
  - (54) Faran Ali, S. M.; Tanwir, F. Oral Microbial Habitat a Dynamic Entity. *J. Oral Biol. Craniofacial Res.* **2012**, 2 (3), 181–187. <https://doi.org/10.1016/j.jobcr.2012.07.001>.
  - (55) Desvarieux, M.; Demmer, R. T.; Jacobs, D. R.; Papapanou, P. N.; Sacco, R. L.; Rundek, T. Changes in Clinical and Microbiological Periodontal Profiles Relate to Progression of Carotid Intima-Media Thickness: The Oral Infections and Vascular Disease Epidemiology Study. *J. Am. Heart Assoc.* **2013**, 2 (6), e000254. <https://doi.org/10.1161/JAHA.113.000254>.
  - (56) Cortelli, J. R.; Barbosa, M. D. S.; Westphal, M. A. Halitosis: A Review of Associated Factors and Therapeutic Approach. *Braz. Oral Res.* **2008**, 22 (SUPPL.1), 44–54. <https://doi.org/10.1590/S1806-83242008000500007>.
  - (57) Lynnerup, N.; Klaus, H. D. *Fundamentals of Human Bone and Dental Biology*; Elsevier Inc., 2019. <https://doi.org/10.1016/B978-0-12-809738-0.00004-1>.
  - (58) Goldberg, M.; Kulkarni, A. B.; Young, M.; Boskey, A. Dentin: Structure, Composition and Mineralization. *Front. Biosci. - Elit.* **2011**, 3 E (2), 711–735. <https://doi.org/10.2741/e281>.
  - (59) Staines, M.; Robinson, W. H.; Hood, J. a. Spherical Indentation of Tooth Enamel. *J. Mater. Sci.* **1981**, 16 (9), 2551–2556. <https://doi.org/10.1007/BF01113595>.
  - (60) Marshall, G. W.; Marshall, S. J.; Kinney, J. H.; Balooch, M. The Dentin Substrate: Structure and Properties Related to Bonding. *J. Dent.* **1997**, 25 (6), 441–458.

- (61) Huang, G. T. J. Dental Pulp and Dentin Tissue Engineering and Regeneration: Advancement and Challenge. *Front. Biosci. - Elit.* **2011**, 3 E (2), 788–800. <https://doi.org/10.2741/e286>.
- (62) Ramsay, S. E.; Whincup, P. H.; Watt, R. G.; Tsakos, G.; Papacosta, A. O.; Lennon, L. T.; Wannamethee, S. G. Burden of Poor Oral Health in Older Age: Findings from a Population-Based Study of Older British Men. *BMJ Open* **2015**, 5 (12). <https://doi.org/10.1136/bmjopen-2015-009476>.
- (63) Gupta, P.; Gupta, N.; Pawar, A. P.; Birajdar, S. S.; Natt, A. S.; Singh, H. P. Role of Sugar and Sugar Substitutes in Dental Caries: A Review. *ISRN Dent.* **2013**, 2013, 1–5. <https://doi.org/10.1155/2013/519421>.
- (64) Buzalaf, M. A. R.; Hannas, A. R.; Kato, M. T. Saliva and Dental Erosion. *J. Appl. Oral Sci.* **2012**, 20 (5), 493–502. <https://doi.org/10.1590/S1678-77572012000500001>.
- (65) Huang, R.; Li, M.; Gregory, R. L. Bacterial Interactions in Dental Biofilm. *Virulence* **2011**, 2 (5), 435–444. <https://doi.org/10.4161/viru.2.5.16140>.
- (66) Eppele, M.; Meyer, F.; Enax, J. A Critical Review of Modern Concepts for Teeth Whitening. *Dent. J.* **2019**, 7 (3), 1–13. <https://doi.org/10.3390/dj7030079>.
- (67) JJ, H. Historical View of Dentifrice Functionality Methods. *J Clin Dent* **1998**, 9 (3), 53–56.
- (68) Rigano, L. Anatomy of Toothpaste Formulas. *Cosmet. Toilet.* **2012**.
- (69) Forward, G. Role of Toothpastes in the Cleaning of Teeth. *Int Dent J* **1991**, 41, 164–170.
- (70) Moharamzadeh, K. *Biocompatibility of Oral Care Products*; Elsevier Ltd, 2017. <https://doi.org/10.1016/B978-0-08-100884-3.00008-4>.
- (71) Nathan, G. K.; Jones, W. J. D. Influence of the Hardness of Abrasives on the Abrasive Wear of Metals. *Arch. Proc. Inst. Mech. Eng. Conf. Proc. 1964-1970 (vols 178-184), Var. titles Label. Vol. A to S* **2006**, 181 (315), 215–221. [https://doi.org/10.1243/PIME\\_CONF\\_1966\\_181\\_317\\_02](https://doi.org/10.1243/PIME_CONF_1966_181_317_02).
- (72) Katoh, T.; Kang, H. G.; Paik, U.; Park, J. G. Effects of Abrasive Morphology and Surfactant Concentration on Polishing Rate of Ceria Slurry. *Japanese J. Appl. Physics, Part 1 Regul. Pap. Short Notes Rev. Pap.* **2003**, 42 (3), 1150–1153. <https://doi.org/10.1143/JJAP.42.1150>.
- (73) Navarre, M. G. *The Chemistry and Manufacture of Cosmetics*; Florida, Orlando, 1975; Vol. 3.
- (74) Schemehorn, B. R.; Moore, M. H.; Putt, M. S. Abrasion, Polishing, and Stain Removal Characteristics of Various Commercial Dentifrices in Vitro. *J. Clin. Dent.* **2011**, 22 (1), 11–18.
- (75) Stookey, G.; Burkhard, T.; Schemehorn, B. R. In Vitro Removal of Stain with Dentifrices. *J Dent Res* **1982**, 61, 1236–1239.
- (76) Grabenstetter, R.; Broge, R.; Jackson, F.; Radlike, A. The Measurement of the Abrasion of Human Teeth by Dentifrice Abrasives: A Test Utilizing Radioactive Teeth. *J Dent Res* **1958**, 37, 1060–1068.
- (77) Schemehorn, B. R.; Ball, T.; Henry, G.; Stookey, G. Comparing Dentifrice Abrasive Systems with Regard to Abrasion and Cleaning. *J Dent Res* **1992**, 71, 559.